Journal of Petroleum Geology, Vol. 41(1), January 2018, pp 5-27

AN INTRODUCTION TO THE PRECAMBRIAN PETROLEUM SYSTEM IN THE SANKURU-MBUJI-MAYI-LOMAMI-LOVOY BASIN, SOUTH-CENTRAL DEMOCRATIC REPUBLIC OF CONGO

F. Delpomdor[1,2*], S. Bonneville[2], K. Baert[3] and A. Préat[2]

This study presents a preliminary assessment of the petroleum potential of the Meso-Neoproterozoic Mbuji-Mayi Supergroup in the Sankuru-Mbuji-Mayi-Lomami-Lovoy Basin in the southern-central Democratic Republic of Congo. This basin is one of the least explored in Central Africa and is a valuable resource for the evaluation of the petroleum system in the greater Congo Basin area. Highly altered carbonates (potential reservoir rocks) and black shales (potential source rocks) are present in the Mbuji-Mayi Supergroup, which can be divided into the BI and overlying BII groups (Stenian and Tonian, respectively). For this study, samples of the BIe to BIIe subgroups from five boreholes and two outcrops were evaluated with petrographic, petrophysical and geochemical analyses.

Carbonates in the BIe to BIIe subgroups with reservoir potential include oolitic packstones and grainstones, stromatolitic packstones and boundstones, various dolostones, and brecciated and zoned limestones. Thin section studies showed that porosity in samples of these carbonates is mainly vuggy and mouldic with well-developed fractures, and secondary porosity is up to 12%. Black shales in the BIIc subgroup have TOC contents of 0.5-1%, and the organic matter is interpreted to have been derived from precursor Type I / II kerogen. The thermal maturity of asphaltite in carbonate samples is indicated by Raman spectroscopy-derived palaeo-temperatures which range from ~150 to ~260°C, which is typical of low-grade metamorphism. Raman reflectance ($R_{mc}R_o$%) values on asphaltite samples were between 1.0 and 2.7%, indicating mature organic matter corresponding to the oil and wet gas windows. Source rock maturation and primary oil migration are interpreted to have occurred during Lufilian deformation (650-530 Ma). The solid asphaltite present in fractures in the dolostones of the BIIc subgroup may represent biodegraded light oil from an as-yet unknown source which probably migrated during the Cambrian-Ordovician (~540-480 Ma). This migration event may have been related to the effects of the peak phase of Lufilian deformation in the Katanga Basin to the SE.

This study is intended to provide a starting-point for more detailed evaluations of potential hydrocarbon systems in the Sankuru-Mbuji-Mayi-Lomami-Lovoy Basin and the adjacent greater Congo Basin area.

[1] Illinois State Geological Survey, University of Illinois, 625 E. Peabody dr., 61820 Champaign, Illinois, USA.
[2] Biogeochemistry and Modeling of the Earth System, Université Libre de Bruxelles, 50 av. F.D. Roosevelt, CP 160/02, 1050 Brussels, Belgium.
[3] Research Group Electrochemical and Surface Engineering, Department Materials and Chemistry, Vrije Universiteit Brussel, Pleinlaan 2, 1050 Brussels, Belgium.
* Corresponding author, email: fdelpomd@illinois.edu

Key words: Precambrian, Congo Basin, petroleum system, asphaltite, bitumen, diagenesis, pyrolysis, source rocks, reservoir rocks, DR Congo.

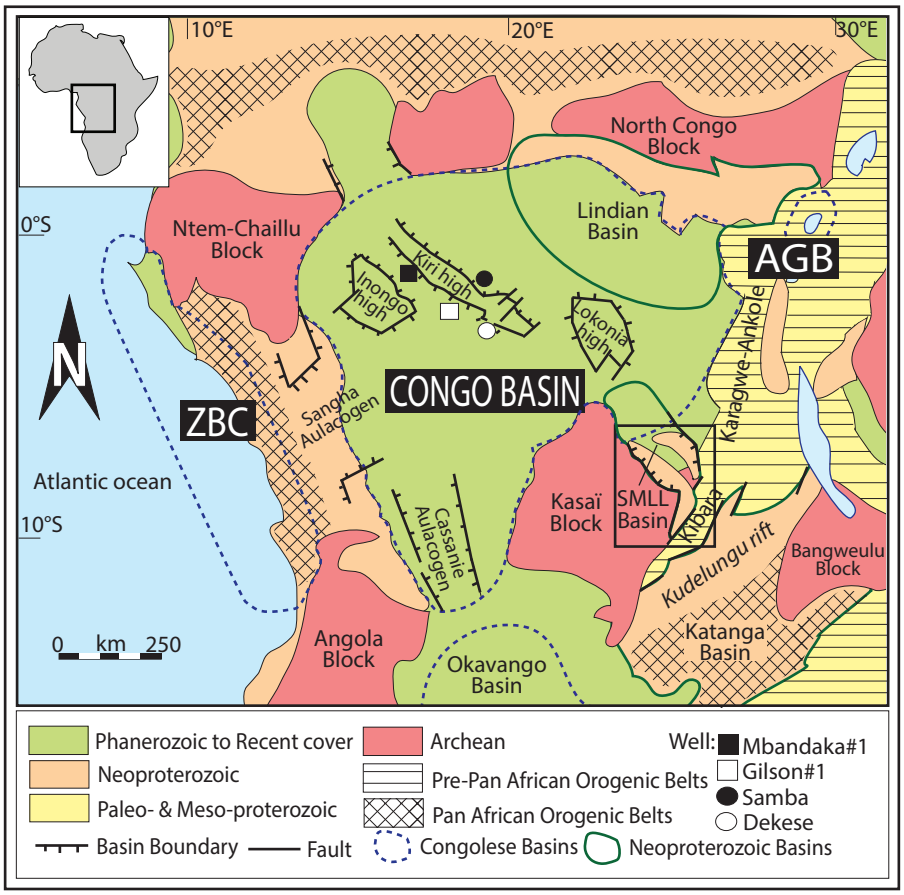

Fig. 1. Outline map of basins with petroleum potential in the Democratic Republic of Congo. ZBC: Zone du Bassin Côtier; AGB: Albertine Graben Basin. The Sankuru-Mbuji-Mayi-Lomami-Lovoy (SMLL) Basin, the focus of this study, is located to the SE of the greater Congo Basin. The petroleum potential of the latter basin has been summarized by Kadima *et al.* (2011a,b), Kadima Kabongo *et al.* (2015) and Delvaux and Fernandez-Alonso (2015). Petroleum systems have been identified in the Lindian and Katanga Basins (Heijlen *et al.*, 2008; Kadima *et al.*, 2011a,b; Sachse *et al.*, 2012; Delvaux and Fernandez-Alonso, 2015).

INTRODUCTION

The Sankuru-Mbuji-Mayi-Lomami-Lovoy (SMLL) Basin is one of the least explored basins in Central Africa, and is a failed rift located to the SE of the greater Congo Basin in the Democratic Republic of Congo (DRC). Exploration of the Congo Basin began with the drilling of the Samba #1 and Dekese #1 wells in the 1950s by REMINA ("Syndicat à la Société belge de Recherches minières en Afrique") and by PETROFINA and FORAKY (see Cahen *et al.*, 1959, 1960) (locations in Fig. 1). Gravimetric and seismic data were acquired over the next 30 years but only two wells (Mbandaka #1 and Gilson #1: Fig. 1) were drilled by the Esso-Shell-Texaco consortium between 1970 and 1984. In general, exploration results were disappointing in terms of commercial hydrocarbon potential.

The petroleum potential of the greater Congo Basin was recently summarized by Kadima *et al.* (2011a,b), Kadima Kabongo *et al.* (2015) and Delvaux and Fernandez-Alonso (2015). No petroleum potential has been identified in the west of the basin, but a petroleum system has been identified in the Lindian and Katanga Basins in the NE and SE respectively (Fig. 1) (Heijlen *et al.*, 2008; Kadima *et al.*, 2011a,b; Sachse *et al.*, 2012; Delvaux and Fernandez-Alonso, 2015). Recent exploration activity in the Lindian Basin on the NE margin of the greater Congo Basin has focused on the organic geochemistry of Infracambrian black shales, which have TOC values ranging between 1.7% and 3% (Lawrence and Makazu, 1988; Daly *et al.*, 1992; Sachse *et al.*, 2012). Volumes of petroleum in-place were estimated to be up to 300 MM brl of oil and 30 Tcf of natural gas (Mello, 2008; Moundounga, 2008). However, Sachse *et al.* (2012) concluded that the shales contain Type III/IV kerogen and as a consequence have little oil source potential.

Recent studies in the SMLL Basin have identified a potential petroleum system with source rocks and carbonate reservoir rocks in the Meso-Neoproterozoic Mbuji-Mayi Supergroup (Fig. 2), sealed by unconformably overlying Permo-Carboniferous glacial sediments and Cretaceous claystones (Delpomdor

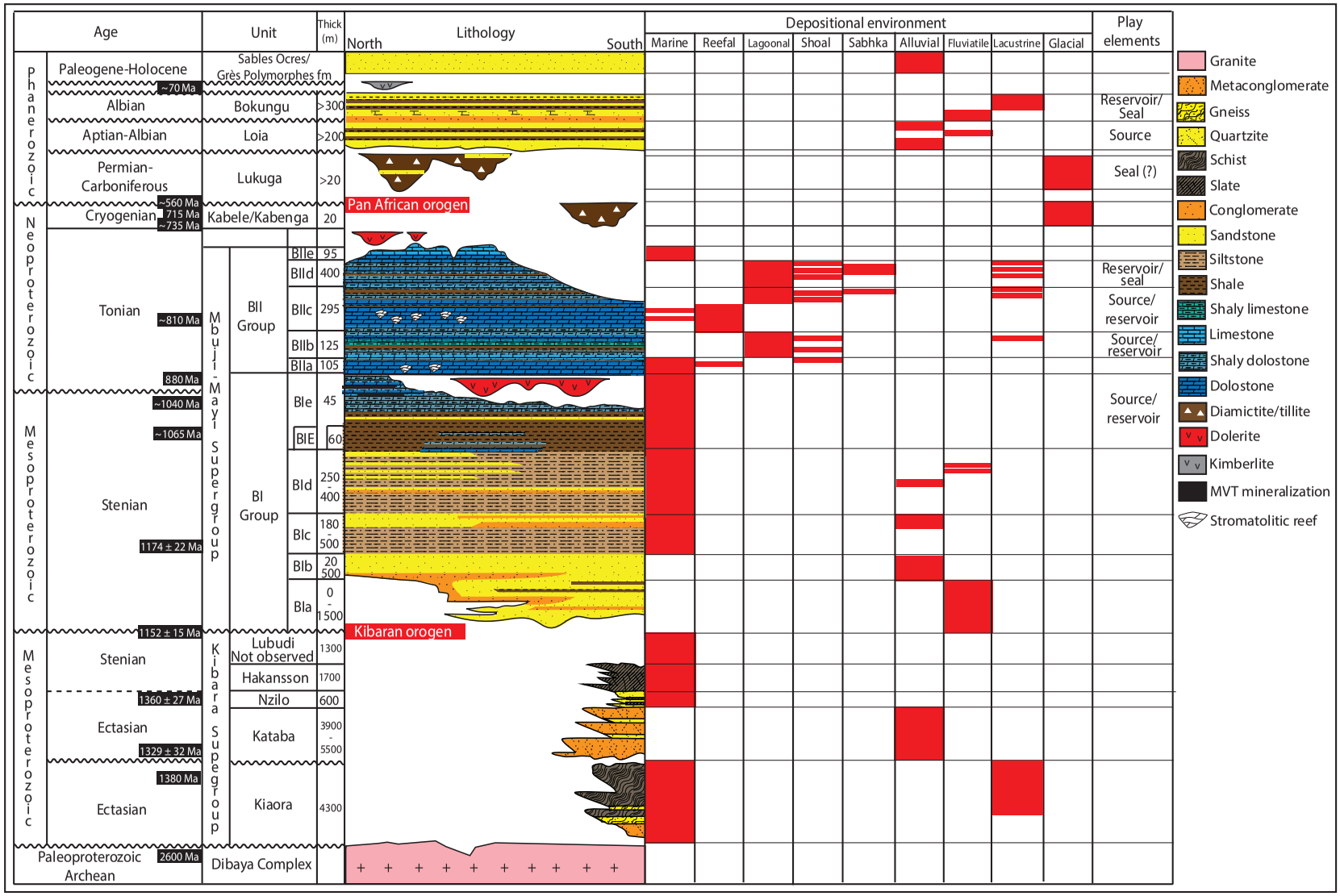

Fig. 2. Chrono- and lithostratigraphic section of the Sankuru-Mbuji-Mayi-Lomami-Lovoy Basin. This study focuses on the BIe to BIIe carbonates and black shales which were deposited in marine and lacustrine environments. Chronostratigraphy is from Cahen (1954), Holmes and Cahen (1955), Delhal *et al.* (1966), Cahen *et al.* (1974, 1984), Maheshwari *et al.* (1977), Delpomdor *et al.* (2013b) and François *et al.* (2017); depositional environments are from Raucq (1957, 1970), Delpomdor *et al.* (2015) and this paper (see text).

and Préat, 2012). The presence of bitumen in fractured carbonates has been recorded in previous studies (Delpomdor and Préat, 2012; Delpomdor *et al.*, 2013a, 2015), but no detailed studies have yet been published. An improved understanding of the diagenetic characteristics of the carbonate reservoir rocks in the Mbuji-Mayi Supergroup, and of the organic geochemistry of the black shales, may help to evaluate the hydrocarbon potential of the SMLL basin, and of the greater Congo Basin area.

The purpose of this study is therefore to investigate potential carbonate reservoir rocks in the Mbuji-Mayi Supergroup, and to determine the petroleum potential and thermal maturity of the black shales. These new data will contribute to a better understanding of the petroleum system in the poorly-explored Congo Basin area.

Regional framework and stratigraphy of the Sankuru-Mbuji-Mayi-Lomami-Lovoy (SMLL) Basin

The evolution of the SMLL Basin began with local uplift related to the far-field effects of the Late Mesoproterozoic Kibaran and Karagwe-Angwole orogenic events along the SE and eastern margins of the Congo Craton. This phase was followed by intracratonic rifting in the Late Mesoproterozoic and Early Neoproterozoic which did not develop into continental break-up, and hence the basin is referred to as a failed rift. Post-rift subsidence was accompanied by the deposition of the thick sedimentary succession of the Mbuji-Mayi Supergroup (Fig. 2), which is overlain by the Cryogenian Kabele and Kabenga Conglomerates. The basin subsequently underwent periods of compression/inversion and rifting, and the Phanerozoic stratigraphy is therefore divided by a series of prominent unconformities (Fig. 2). Thus, the Kabele and Kabenga Conglomerates are unconformably overlain by the Late Carboniferous – Permian Lukuga diamictites (Fig. 2) above which are unconformity-bound Aptian-Albian and Albian successions.

The geochronology of the Mbuji-Mayi Supergroup has been investigated by Cahen (1954), Holmes and Cahen (1955), Delpomdor and Préat (2013), Delpomdor *et al.* (2013b), Baludikay *et al.* (2016a), and François *et al.* (2017). The Supergroup was deposited between ~1155 and ~810 Ma and is divided into the Stenian BI group and the overlying Tonian BII group, each of which is divided into lithostratigraphic subgroups (BIa-e and BIIa-e respectively, Fig. 2). At the base of the BI group are the transgressive fluviatile quartz arenites and shales of the ~1155-1100 Ma BIa and BIb subgroups (Fig. 2) in the southern margin of the craton, which are overlain by alluvial to marine conglomerates, argillaceous sandstones and shales of the ~1100-1060 Ma BIc and BId subgroups (Raucq, 1970; Delpomdor *et al.*, 2013b). Marine sandstones of the ~1060-1000 Ma BIe subgroup are present throughout the basin (Raucq, 1970).

Differential subsidence occurred throughout the basin in the Late Stenian. Deep-marine conditions occurred in the area around Luembe (Fig. 3) in the centre of the basin. Shales, sandstones and calcareous dolostones of the BIE subgroup were deposited, while the margins of the basin recorded shallow-marine sediments including the sandstones and shale-rich dolomites of the BIe subgroup (Raucq, 1970; Delpomdor *et al.*, 2015).

The galena mineralization (with conventional $^{207}Pb/^{206}Pb$ ages of 1040 and 1065 Ma; Cahen, 1954; Holmes and Cahen, 1955) recorded at various locations, and dolerite intrusions at the transition between the BI and BII groups, were controlled by a fault system related to the continental break-up of Rodinia and the opening of the Adamastor ocean along the southern and western margins of the Congo Craton starting at ~1000 Ma (Tack *et al.*, 2001; Raucq, 1957, 1970). The SMLL Basin then became more stable with the deposition of the transgressive dolostones, stromatolitic carbonates and oolitic shoals of the ~1100-810 Ma BIIa and BIIb subgroups (Fig. 2) (Raucq, 1957, 1970; Delpomdor *et al.*, 2013b, 2015). Deposition of black shales, evaporites and caliche occurred in sabkhas and isolated lakes (Delpomdor *et al.*, 2013a,b, 2015). A regional transgression at ~810 Ma was accompanied by the deposition of the dolostones of the BIIc subgroup in marginal parts of the basin, while organic-rich black shales accumulated in more internal areas (Delpomdor *et al.*, 2013b, 2015). The overlying BIId subgroup dolostones with oolitic and organic-rich intervals were deposited in marine to lacustrine environments (Raucq, 1957; 1970; Delpomdor *et al.*, 2015).

In response to rapid subsidence of the Kundelungu rift in the Katanga Basin to the SE of the SMLL Basin (Fig. 1), continental glaciation occurred in the elevated rift margins (recorded by the 735-715 Ma Sturtian glaciation), with the deposition of the Cryogenian Kabele and Kabenga Conglomerates in the extreme south of the basin and the Grand Conglomérat Formation in the Katanga Basin (Cahen and Mortelmans, 1947). A 200 Ma depositional hiatus then occurred in the SMLL Basin and was related to the Cryogenian–Ediacaran amalgamation of eastern Gondwana. During the ~750-560 Ma time period, the São Francisco-Congo craton was assembled with the Arabian–Nubian Shield together with the Indian, Madagascan, East Antarctica and Australian cratons (Fitzsimons, 2000; Meert, 2003). The stratigraphic hiatus (Fig. 2) suggests that the basin was uplifted during this time interval.

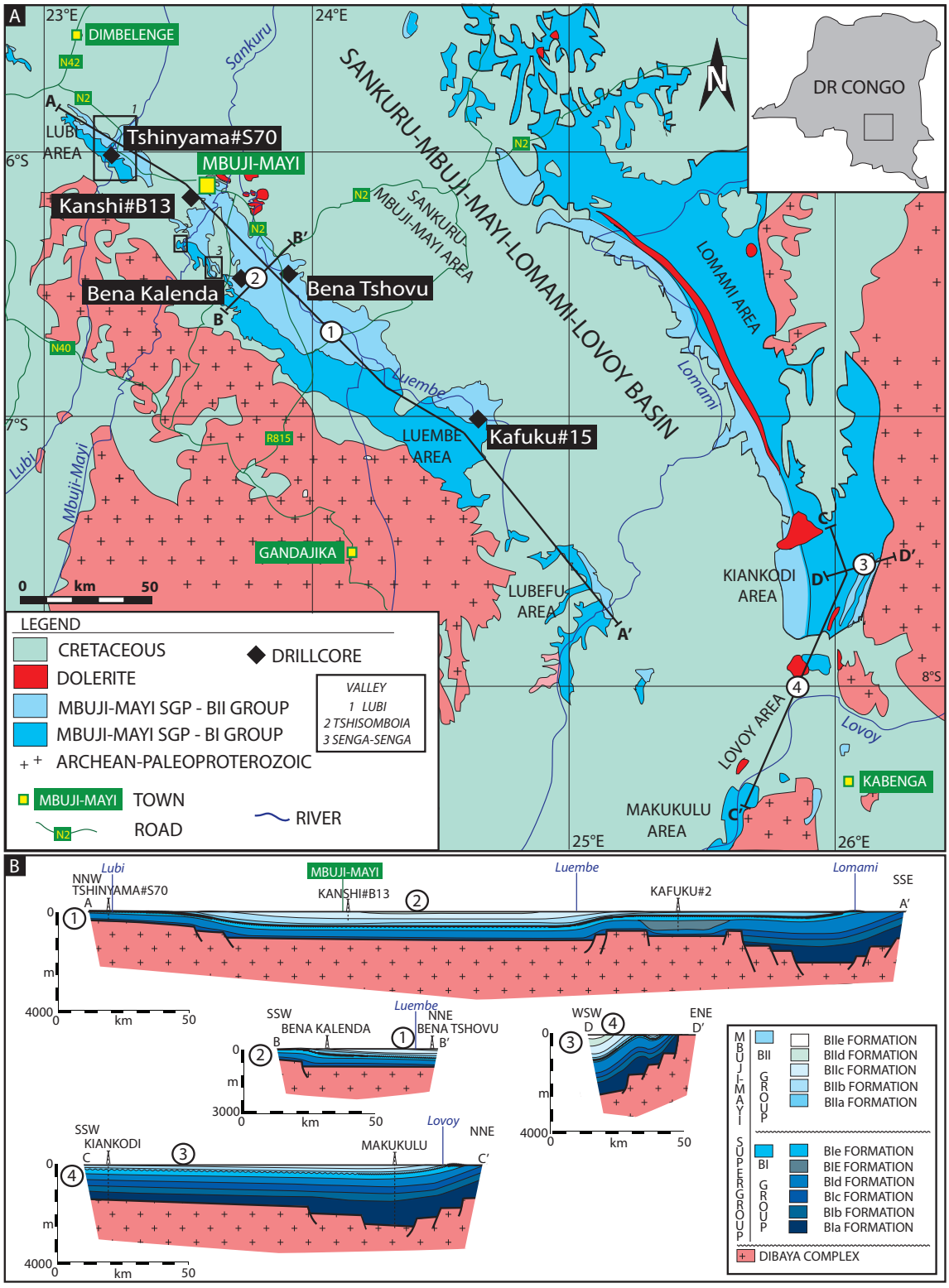

Fig. 3. (A) Simplified geological map of the Sankuru-Mbuji-Mayi-Lomami-Lovoy Basin in the Democratic Republic of Congo (see Fig 1), showing the location of the five studied boreholes and the two outcrops intersecting the BIe-BIIe subgroups.
(B) Cross-sections of the Mbuji-Mayi succession which rests on Archean crystalline basement or on the Kibaran Supergroup in the SMLL Basin (profile lines are shown in Fig. 3A). Cross-sections A-A' and B-B' show a tabular Mbuji-Mayi succession resting on Archean basement; well Kafuku #15 in the Luembe area penetrates the BIe subgroup. Cross-section C-C' shows that the Mbuji-Mayi succession in the Kiankodi area is folded, with dips of up to 60° (Cahen and Mortelmans, 1947). Cross-section D-D' shows that the succession in the Makukulu area is folded with dips of 10-40°, and that it rests uncomformably on the Kibaran Supergroup (Cahen and Mortelmans, 1947). Raucq (1970) suggested that the basin succession in general deepens to the south.

The major regional unconformity at the base of the Upper Carboniferous – Permian Lukuga Group (Fig. 2) records the drift of Gondwana during the Late Devonian – Mid Carboniferous (Torsvik and Cocks, 2011). The Lukuga Group consists of glacial polymictic tillites associated with periglacial sandstones and argillites deposited in local depressions or palaeo-glacial valleys (J. Hielsma, 2010, AngloAmerican, *pers. comm.*).

A regional-scale unconformity separates the Palaeozoic and possibly the Triassic from the Jurassic–Cretaceous successions (Delvaux and Fernandez-Alonso, 2015). This hiatus is attributed to compressional inversion in the Congo Basin (Daly *et al.*, 1992) and regional uplift in the SMLL Basin. Compression was related to the far-field effects of the Cape Fold Belt in South Africa during the Late Permian – Triassic (Delvaux and Fernandez-Alonso, 2015), and the rifting of the South Atlantic Ocean during the Triassic – Late Jurassic (Heine *et al.*, 2013). In the SMLL Basin, the Lower Cretaceous Loia Group consists of lacustrine argillaceous and calcareous sandstones, argillites and marls including thin conglomerates and black shales (Maheshwari *et al.*, 1977; Delhal and Ladmirant, 1979; Linol *et al.*, 2015). These are overlain by the Lower Cretaceous fluvio-deltaic Bokungu Group composed of sandstones and argillites (Maheshwari *et al.*, 1977; Delhal and Ladmirant, 1979; Colin, 1994). Uplift of the basin was accompanied by the intrusion of syn-rift chromiferous kimberlites (120-70 Ma) at locations between the Lubi and Mbuji-Mayi rivers (Fig. 1) (Fieremans, 1977; Demaiffe and Fieremans, 1981; Demaiffe *et al.*, 1991).

Paleogene and Pleistocene sedimentation in the SMLL Basin corresponds to the uplift and weathering of the Congo Basin. The detrital "Grès Polymorphes" and "Sables Ocres" formations consist of Paleogene and Pleistocene alluvial and lacustrine or continental sands respectively (Cahen *et al.*, 1959, 1960; Delhal and Ladmirant, 1979).

Potential petroleum system elements

Source rocks

Petroleum systems in the SMLL Basin are poorly understood due to a lack of data. Potential source rock intervals in the SMLL Basin are located in the Meso-Neoproterozoic, Permo-Carboniferous and Cretaceous successions (Lawrence and Makazu, 1988; Daly *et al.*, 1992; Sachse *et al.*, 2012; Delvaux and Fernandez-Alonso, 2015).

Early Neoproterozoic black shales in the BII group of the Mbuji-Mayi Supergroup are the focus of this study. The black shales dominantly contain cyanobacterial and acritarch-derived organic matter (OM) (Maithy, 1975; Baudet, 1987; Baludikay *et al.*, 2016a), together with fungal-derived lagoonal and lacustrine OM (Delpomdor and Préat, 2012; Bonneville *et al.*, 2015). Petrographic studies have indicated the presence of kerogen within the stromatolites of the BIIc subgroup, and degraded bitumen within fractured carbonates in the BII group (Delpomdor and Préat, 2012). However, *n*-alkane and biomarker patterns in samples of the black shales from the Mbuji-Mayi Supergroup could not be identified in previous studies of archived core samples as a consequence of long-term storage (and oxidation) at the Royal Museum for Central Africa (Belgium) (N. Gueneli, 2012, Australian National University, *pers. comm.*).

Organic-rich Permo-Carboniferous and Cretaceous shales from the SMLL Basin have not been analyzed petrographically or in terms of organic geochemistry. However, equivalent units from the Congo Basin have been studied. In the Congo Basin, the Permo-Carboniferous peri-glacial shales of the Lukuga Group have TOC values of < 2.4% and contain Type III-IV gas-prone kerogen (Rock-Eval T_{max}: 410-455˚C), with little hydrocarbon generation potential (Delvaux and Fernandez-Alonso, 2015). Hydrogen and oxygen indexes range between 5-158 and 22-235 mg HC/g C_{org}, respectively (Sachse *et al.*, 2012). Lacustrine black argillites in the Cretaceous Loia Formation (Congo Basin) have TOC contents up to 25% and are considered to have good to excellent source rock potential with Type I/II kerogen (Rock-Eval T_{max}: 430-450˚C), and hydrogen and oxygen indexes of ~800 mg and 50-60 mg HC/g C_{org}, respectively (JNOC, 1984; Sachse *et al.*, 2012). The Loia Group shales contain algal-derived aquatic organic matter with minor amounts of terrigenous higher plant material (Sachse *et al.*, 2012; Delvaux and Fernandez-Alonso, 2015).

Seepage oils from the Congo Basin contain a high concentration of angiosperm-derived oleanane indicating an Early Cretaceous to Tertiary age for the source rock (Mello, 2008).

Reservoir rocks

Potential reservoir rocks in the SMLL Basin include a range of carbonates and siliciclastics of ages varying from Meso-Neoproterozoic to Cretaceous, which in general have been little studied. Carbonates with reservoir potential are present in the BI and BII groups of the Mbuji-Mayi Supergroup, and the siliciclastic rocks of the Aptian-Albian Bokungu Group are also considered to have reservoir potential (Delvaux and Fernandez-Alonso, 2015).

In the Congo Basin, Mello (2008) identified four potential reservoir rocks: (i) the late Neoproterozoic Ituri carbonates; (ii) the Cambro-Ordovician (unnamed) red beds; (iii) the Permo-Carboniferous Lukuga siliciclastics; and (iv) the upper Karoo siliciclastics. None of these potential reservoir rocks are known to occur in the SMLL Basin.

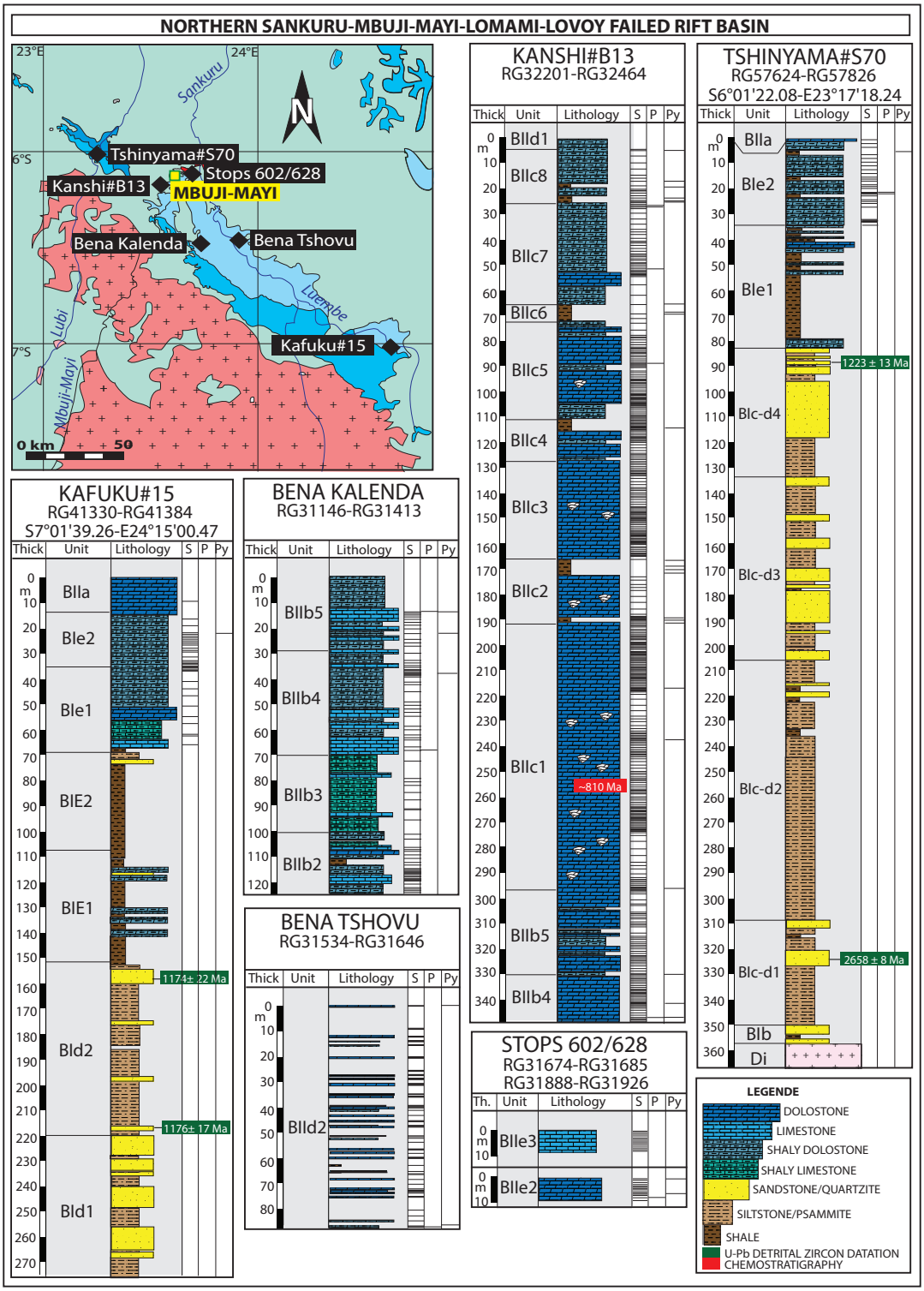

Fig. 4. Location and litho-logs for the five boreholes and two outcrops studied in the northern Sankuru-Mbuji-Mayi-Lomami-Lovoy Basin, showing the stratigraphy of the Mbuji-Mayi Supergroup. Cores and outcrop samples have been stored in the Royal Museum for Central Africa (Tervuren, Belgium) since 1960. Carbonates of the BIe to BIIe subgroups were sampled from wells Tshinyama #S70 (BIe_{1-2} formations, samples RG57624–57826); Bena Kalenda ($BIIb_{2-5}$ formations, samples RG31146-31413); Kanshi #B13 ($BIIb_4$ to $BIIc_8$ formations, samples RG32201-32464), and Bena Tshovu ($BIId_2$ formation, samples RG31534-31646) in the Sankuru/Mbuji-Mayi area; from well Kafuku #15 (BIe_1 formation, BIIa subgroup; samples RG41330–41384) in the Luembe section. Samples from two outcrops intersecting the $BIIe_{2-3}$ formations (Stops 602/628, samples RG31674-31685 and RG31888-31926) were also analyzed. Abbreviations: S, sample and petrography; P, porosity and permeability; Py, Rock-Eval pyrolysis. RG is "Registre Géologique" followed by the Royal Museum for Central Africa sample serial number.

In this study, we investigate the reservoir potential of carbonates from the BII group, including oolitic carbonates in the BIIc and BIId subgroups, and stromatolitic carbonates in the BIIc subgroup. Stromatolitic bioherms in the BIIc subgroup (Bertrand-Sarfati, 1972) may have formed a depositional barrier with the accompanying development of a restricted, probably lagoonal environment in which there was episodic evaporite precipitation (Delpomdor *et al.*, 2015). BIIc dolomites contain black shale intercalations and bitumen in fractures which were analyzed to evaluate their source rock potential.

Seals, traps

Potential seals are fine-grained carbonates and evaporitic intervals (e.g. in the BIId subgroup) in the BII group, or unconformably overlying Permo-Carboniferous Lukuga and Cretaceous Loia siliciclastics.

Structural traps in the SMLL Basin are not known, although compressional structures such as anticlines and thrusts have been observed along the SE margin of the basin (Cahen and Mortelmans, 1947).

MATERIALS AND METHODS

Samples

This study is based on cores and outcrop samples from seven locations in the SMLL Basin (Figs 3, 4). Cores from five boreholes were studied: the boreholes were Tshinyama #S70 in the Lubi area in the NW (Fig. 3); Bena Kalenda, Kanshi #B13 and Bena Tshovu in the Sankuru/Mbuji-Mayi area; and Kafuku #15 in the Luembe area to the SE (Fig. 3). All cores were stored in the Geological Department of the Royal Museum for Central Africa (Tervuren, Belgium). In addition, samples from two outcrops were studied: Stops 602 and 608 to the east of the town of Mbuji-Mayi (Fig. 4). These samples were also stored in the collection of the Royal Museum for Central Africa. The Museum identifies samples with the code "RG" (Registre Géologique) followed by a serial number. All samples came from the BIe to BIIe subgroups of the Mbuji-Mayi Supergroup.

Potential reservoir rocks

Borehole samples consist of carbonates from the BIe subgroup and the BII group (Fig. 4). At the Tshinyama #S70 well, samples RG 57624–57826 came from the BIe_{1-2} to BIIa interval (Fig. 4). Samples from Bena Kalenda well (RG 31146-31413) came from the $BIIb_{2-5}$; those from Kanshi #B13 well (RG 32201-32464) from the $BIIb_4$ to $BIIc_8$; and those from Bena Tshovu well (RG 31534-31646) from the $BIId_2$. At the Kafuku #15 well, samples came from the BIe_1-BIIa interval (RG 41330–41384) (Fig. 4). A total thickness of ~525 m of core was analyzed in detail and 755 carbonate samples were collected from split cores (10 cm in diameter) at sampling intervals of ± 0.3 m.

Thirty-three outcrop samples from Stops 602 and 628 (samples RG 31674-31685 and RG 31888-31926; Fig. 4) were recovered from the $BIIe_{2-3}$ interval.

Brief descriptions of these samples were given by Raucq (1957, 1970) and Delpomdor *et al.* (2013b, 2015). Lithology, sedimentary structures, porosity and permeability were measured from the core and outcrop samples, and depositional environments were interpreted (Delpomdor *et al.*, 2013a; 2015). In addition, carbonate samples were studied for their diagenetic characteristics (see results in Table 1).

Potential source rocks

Thirty-four samples from the BIe to BIIe subgroups were analyzed for their source rock potential. Organic-rich carbonates including dolostones and dolomitic limestones together with black shales and bitumen (asphaltite) inclusions in dolostones were selected for geochemcial analysis due to their enrichment in organic matter, based on observations of cores and thin sections. Samples of dolostone from the marine BIe subgroup (n = 2) came from the Tshyniama #S70 and Kafuku #15 wells, and from the lacustrine $BIId_2$ interval (n = 2) from the Bena Tshovu well. Twelve dolostones, ten black shales and three asphaltite inclusions from the marine to lacustrine $BIIb_4$-$BIIc_8$ intervals were sampled from the Kanshi #B13 well cores. Two limestones were selected in the marine $BIIe_2$ formation from the Stop 602 outcrop samples. The samples were analyzed by Rock-Eval pyrolysis to assess their petroleum potential; asphaltite inclusions were also pyrolysed and the results compared with the analyses of potential source rocks, i.e. carbonates and black shales. Results are presented in Table 3.

Methods

X-ray microdiffractometry (Bruker Siemens instrument) and X-ray fluorescence analysis (with a Si-PIN detector from AMPTEK) were carried out on 18 and seven samples respectively, at the Université Libre de Bruxelles (Belgium) to determine the mineralogy and distribution of phyllosilicates, silicates, carbonates and sulphates. Matrix material and cements in 16 samples from the BIe-BIId subgroups were investigated using cathodoluminescence microscopy (Technosyn Cold Cathodoluminescence Model 8200 MkII), at 16-20 kV and 6.65 Pa at the Katholieke Universiteit Leuven (Belgium), and with a JEOL JSM-6100 Scanning Electronic Microscope (SEM) coupled with a EDAX CDU-LEAP detector with an accelerating voltage and amperage of 15 kV and 30 nA at the Université Libre de Bruxelles. Porosity and permeability data were obtained from 10 core samples

Table 1. Description and interpretation of the matrix and cements within the BIe-BIIe carbonates of the Mbuji-Mayi Supergroup.

Phase		Description	Interpretation
Dolomite-I	DOL-I	matrix; tightly packed, equigranular xeno- to hypidiotopic dolomicrite (5-10 µm) in non-planar fabrics; mimetic fabric-preserving rhombs of dolomite; undulatory extinction	shallow and early burial diagenesis
Dolomite-II	DOL-II	matrix; neomorphic hypidiotopic dolomicrosparitic crystals (10-15 µm) in sutured mosaic planar-e fabrics; remnants of primary dolomicrite	shallow and early burial diagenesis
Dolomite-III	DOL-III	matrix; hightly packed, inequigranular, hypidiotopic crystals (30-80 µm), in mosaic fabrics; whitish internal texture with an unit extinction	mixed-water early burial diagenesis
Dolomite-IV	DOL-IV	matrix; loosely packed, equigranular and rhombic hypidio- and idiotopic crystals (50 to >100 µm) in mosaic and sucrosic fabrics	mixed-water early burial diagenesis
Anhydrite-I	ANH-I	pseudomorphs of evaporitic crystals (gypsum, halite and anhydrite) in subvertical lenticular, lozenge-shaped, swallow-tail twins, randomly oriented platy rectangular laths, castle-shaped nodules and coalescent nodular fabrics in chicken-wire structures or in contorted coalescent nodules (enterolites) and evaporitic grain-supported breccias with replaced halite pyramidal hopper structures; replaced by DOL-I to DOL-III	shallow to early diagenesis with precipitation of evaporites in highly saline environments
Anhydrite-II	ANH-II	cement; interlaminated palisadic crusts consisting of bands of vertically oriented chevron-like structures reminiscent of evaporitic crystals	shallow to early diagenesis with precipitation of evaporites in highly saline environments
Anhydrite-III	ANH-III	cement; satin spar; replaced vertical fibrous gypsum crystals; filling pores and fractures	dissolution and remobilization of the evaporites during a possible exhumation of the basin or related to circulation of hydrothermal fluids
Calcite-I	CAL-I	cement; fine to medium needle-like crystals (10-50 µm) normal to substrate	replacement of evaporites during the saline reflux from the hypersaline shelf lagoon and sabkha
Calcite-II	CAL-II	cement; medium- to coarse-grained elongate xenotopic fibers (10-50 µm); sweeping extinction; individual and coalescent dome-shaped hemispheres with radiating fibrous crystals	replacement of evaporites during the saline reflux from the hypersaline shelf lagoon and sabkha
Calcite-III	CAL-III	cement; sutured inequigranular xenotopic mosaics of single crystals (50 to up 200 µm) forming an intracrystalline radiaxial fibrous fabric; straight extinction, with undulate extinction of elongate single crystals	replacement of evaporites during the saline reflux from the hypersaline shelf lagoon and sabkha
Calcite-IV	CAL-IV	cement; alternating light and dark crenulated bands of elongate crystals	replacement of evaporites during the saline reflux from the hypersaline shelf lagoon and sabkha
Dolomite-V	DOL-V	cement; equant crystals (50 to up 200 µm); filling interparticular spaces	shallow to intermediate burial diagenesis
Dolomite-VI	DOL-VI	cement; non-planar idiotopic zoned crystals (100 to up 300 µm); alternations of dark thin zoned non-ferroan and light ferroan dolomite; corroded surface; filling interparticular spaces (vugs, veins, fractures, pores); associated with bitumen	deep burial or hydrothermal diagenesis from high-saline brines and high temperatures, or as a by-product of thermochemical sulfate-reduction
Dolomite-VII	DOL-VII	cement; elongate, xeno- to hypiodiotopic dolomite crystals; straight extinction; filling interparticular spaces (vugs, veins, fractures, pores)	deep burial or hydrothermal diagenesis from high-saline brines and high temperatures, or as a by-product of thermochemical sulfate-reduction
Silica	SI	cement; equigranular crypto- (<4 µm), micro- (4-25 µm) and megacrystalline quartz in porphyrotopic, poikilotopic and mosaic fabrics; replacement of matrix (DOL-I to DOL-IV) and cements (DOL-IV to DOL-VII)	meteoric water invasions into fractures caused precipitation of silica from weathered silicate rocks or silica contributions (hydrothermal source) transported in relatively restricted basin

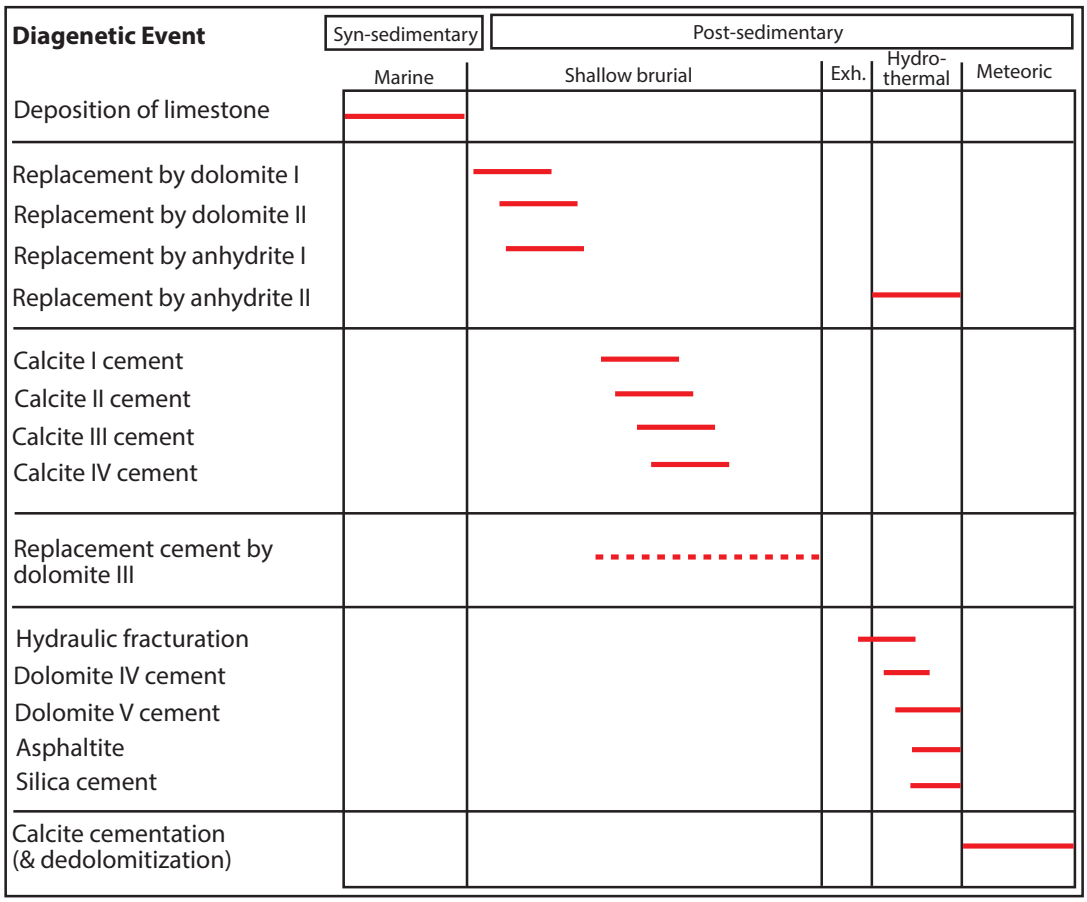

Fig. 5. Paragenetic sequence for the Mbuji-Mayi Supergroup carbonates (see text for details).

from the BIe, BIIb, BIIc and BIId subgroups with an autopore IV 9500 mercury porosimeter at a pressure of ~4 MPa at the Laboratory of Material Sciences in the Université Libre de Bruxelles.

TOC and carbon isotopes were investigated on 33 organic-rich carbonate and black shale samples from the BIe to BIIe subgroups. Analyses were carried out on a LECO carbon analyzer (CS-244) and a Carlo Erba EA1110 elemental analyzer coupled to a mass spectrometer (ThermoFinnigan delta plus XP), at Parma University (Italy). Carbon isotope compositions were calibrated with inter-laboratory standards: sucrose IAEA-CH-6, oil NBS-22 and graphite USGS-24. Organic carbon isotope values are reported in the $\delta^{13}C$ notation normalized to the PDB standard (V-PDB, Vienna Pee Dee Belemnite). The overall precision of carbon isotope analyses is within 0.2‰ (1σ).

Pyrolysis was performed on ten samples with a Rock-Eval VI instrument in the laboratory of Total S.A. (France) to quantify the total organic carbon content as well as the proportions of hydrocarbon and oxygenated components in the organic matter.

Microthermometric analyses of fluid inclusions were performed on five samples recovered from the BIIc subgroup from well Kanshi #B13. Analyses used a Linkham THMSG600 heating–cooling stage and were carried out at the Katholieke Universiteit Leuven (Belgium). Reproducibility was within 0.5 and 5°C for T*m* and T*h* values, respectively.

Visible bitumen inclusions within three thin sections of carbonates of the the BIIc subgroup were analyzed by Raman spectroscopy (LabRAM HR Evolution HORIBA Scientific instrument equipped with a solid state laser at 532nm using a long working distance 50X objective). Spectra were collected at low laser intensity (typically 1%) in order to avoid "amorphisation" artefacts. Peak deconvolution of spectra was performed using *Fytik 0.9.8* (Wojdyr, 2010).

RESULTS

Reservoir rock potential

The BIe to BIIe subgroups contain potential reservoir rocks including oolitic packstones and grainstones, stromatolitic packstones and boundstones, various dolostones, and brecciated and zoned limestones resulting from early diagenesis related to the evaporitic (sabhka) depositional setting. These potential reservoir rocks are mostly present in samples from the BIIc subgroup, where vuggy microporosity and intercrystalline porosity are common in dolomitized stromatolitic boundstones.

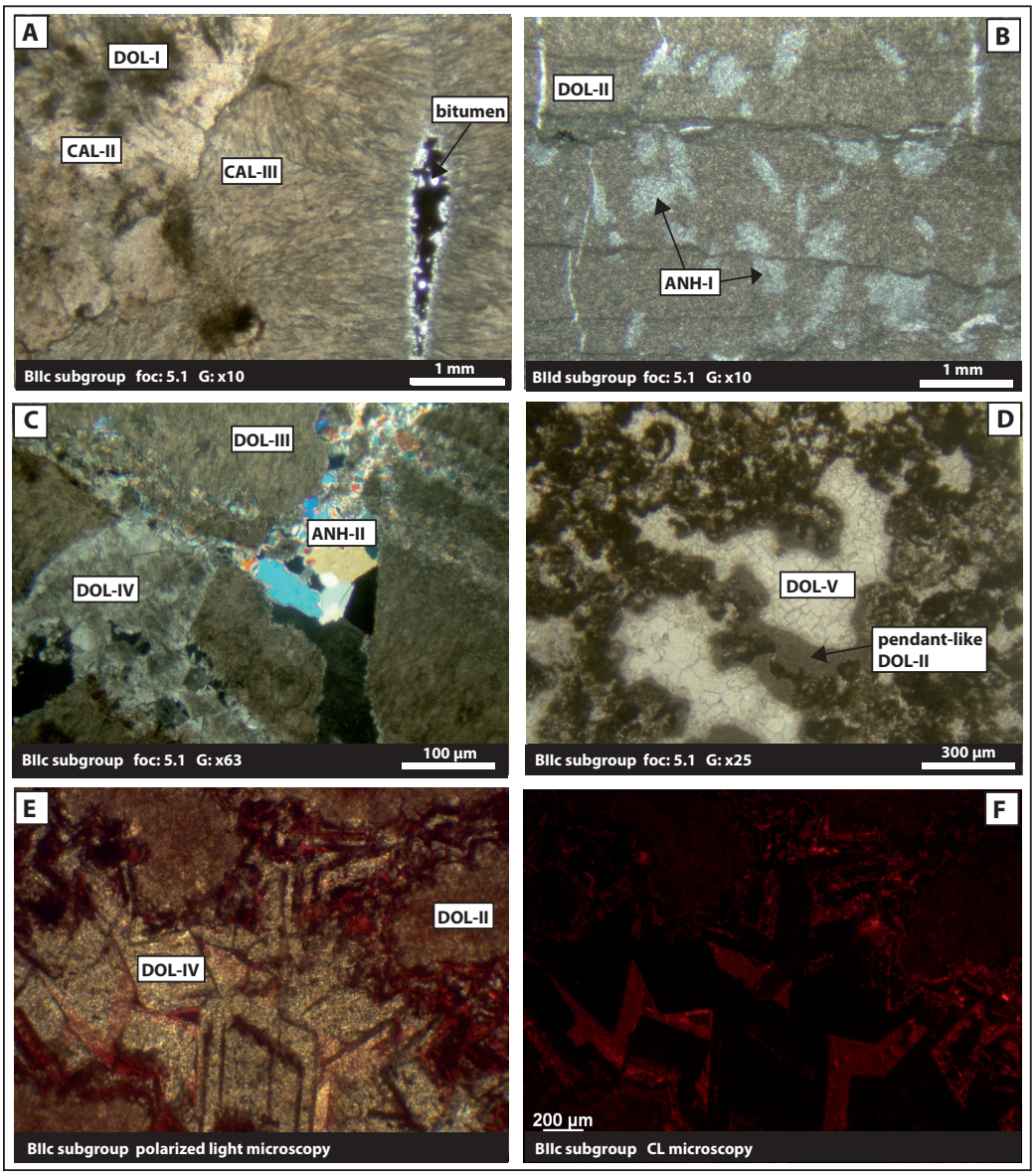

Fig. 6. Photomicrographs showing diagenetic and petrographic characteristics of samples from the BII carbonates:
(A) Dolomicritic stromatolite clots (DOL-I) rimmed by multiple calcite cement phases (botryoidal and spherulitic; CAL-II and CAL-III) replaced by dolomite. Note the presence of dark, pore-filling bitumen in the "interparticle" porosity (mcBC). Well Kanshi #B13 core, BIIc subgroup.
(B) Hypidiotopic dolomicrospar (DOL-II) associated with lozenge-shaped and platy rectangular laths of former anhydrite, after gypsum, replaced by dolomicrospar. Bena Tshovu drill core, BIId subgroup.
(C) Fracture-filling gypsum replaced by anhydrite (ANH-II) and saddle dolospar (DOL-IV) in stromatolitic facies. Well Kanshi #B13 core, BIIc subgroup.
(D) Equant crystalline dolomitic cements (DOL-III) filling the intraparticle spaces in microbial facies. Note the presence of pendant beard-like dolomicrosparitic crystals. Well Kanshi #B13 core, BIIc subgroup.
(E) Plane-polarized light microview of fracture-filling saddle dolomite (DOL-VI), and (F) same view under CL: concentric zonations with multiple zones parallel to growth surfaces show alternating bright red and dark CL colours. Well Kanshi #B13 core, BIIc subgroup.

Cement fabrics

The matrix in the analyzed carbonate samples from the BIe to BIIe subgroups consists of tightly packed neomorphic dolomicrosparite crystals, and petrographic observations indicate a complex diagenetic history with multiple generations of dolomite, anhydrite and calcite cements (Table 1, Fig. 5). The earliest dolomitic phases (DOL-I and DOL-II) are non-luminescent or show a brown/red dull luminescence suggesting reducing conditions (Figs 6G, H). Early anhydrite (ANH-I) was also observed (Fig. 6B).

Four types of calcite cements – fibrous (CAL-I), botryoidal (CAL-II), spherulithic (CAL-III) and herringbone *sensu stricto* (CAL-IV), the latter

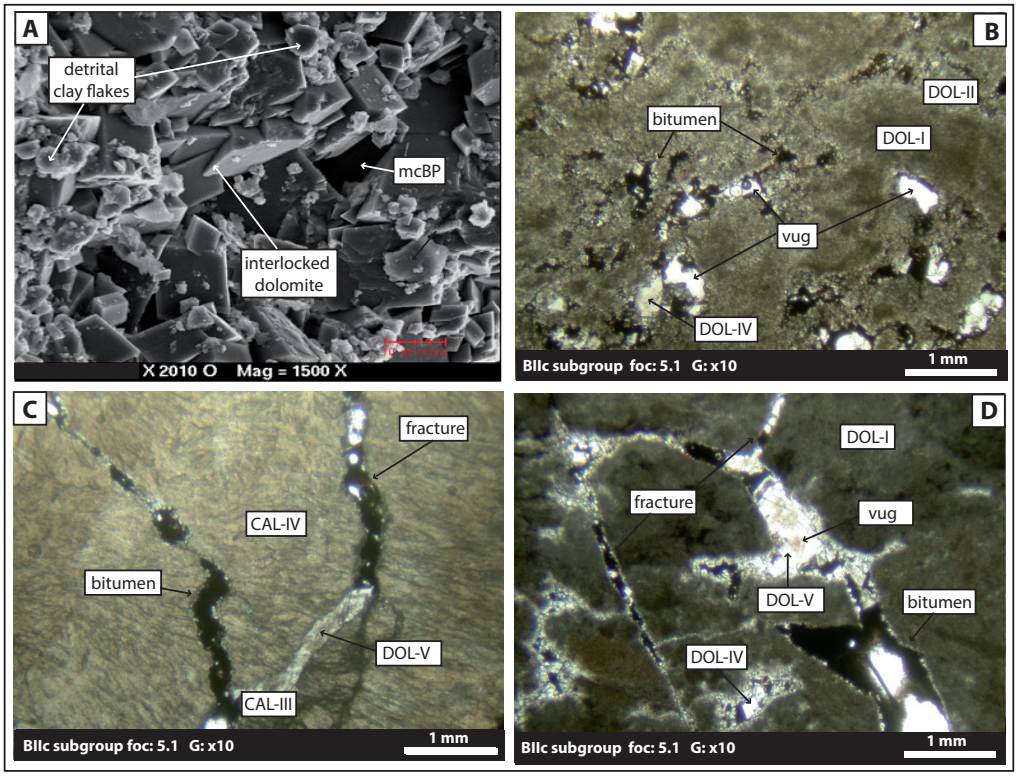

Fig. 7. Photomicrographs showing types of pore spaces in samples from the BII carbonates.
(A) Interlocked dolomite grains forming matrix with detrital clay flakes. Note micropores <1 µm and ~10 µm. Well Kanshi #B13 core, BIIc subgroup.
(B) Vuggy micropore (mcVUG) filled partially by DOL-IV and amorphous bitumen in a stromatolitic facies. Well Kanshi #B13 core, BIIc subgroup.
(C) Fracture microporosity (mcFR) occluded by DOL-V and bitumen in CAL-IV. Well Kanshi #B13 core, BIIc subgroup.
(D) Stromatolitic breccia with fractures and vugs. Well Kanshi #B13 core, BIIc subgroup.

consisting of alternating light and dark crenulated bands less than 1 mm thick (Sumner and Grotzinger, 1996) – were recognized in the stromatolitic facies of the BIIc subgroup in the core samples from well Kanshi #B13. CAL-I cement consists of needle-like calcite crystals growing normal to the substrate. CAL-II calcite comprises elongate radiating fibrous crystals and crystal fans with coalescent dome-shaped hemispheres (Fig. 6A). CAL-III consists of sutured inequigranular xenotopic mosaics of single calcite crystals forming an intracrystalline radiaxial fibrous fabric (Fig. 6A). CAL-IV consists of crenulated bands of elongate calcite crystals. Remnants of calcite cements (CAL-I to CAL-IV) with a high Fe^{2+} content exhibit a weak brown/red "dull" luminescence to non-luminescence (Fig. 6C, D).

Equant dolomite cement crystals (DOL-III, Fig. 6C) fill interparticular spaces and replace anhydrite (ANH-I). DOL-III dolomite exhibits a weak brown/red "dull" luminescence to non-luminescence. Subsequent generations of dolomite cement consist of void- and pore-filling saddle (DOL-IV) and drusy dolomite (DOL-V). DOL-IV shows alternating zones of dark, non-ferroan and light ferroan dolomite (Fig. 6C). This cement displays a weak luminescence sometimes with multiple ("spin-dry") zonations (minimum two phases) with alternating bright red and dark colours, rarely red-orange, indicating alternating Mn^{2+} substituted by Mg^{2+} and Fe^{2+}-rich layers during crystal growth (Figs. 6G, H). DOL-V dolomite, consisting of equant to elongate crystals filling interparticular pores, vugs and fractures (Fig. 6D), is non-luminescent or rarely has a bright red cathodoluminescence, suggesting a change from reducing to oxidizing conditions.

Traces of goethite and haematite were identified within DOL-IV and DOL-V. Anhydrite satin spar (ANH-II) fills pores and fractures (Fig. 6C), and is followed by later, pervasive, equigranular crypto-, micro- and megacrystalline quartz (SI) with porphyrotopic, poikilotopic and mosaic fabrics. These latter cements replaced evaporitic minerals, dolomicritic matrices and cements.

Pore space characterization

Pore space measured in samples of carbonates from the BIe to BIIe subgroups is relatively limited in mud-supported textures and represents less than 10% in grain-supported textures. Crystal edges of DOL-I

Table 2. Porosity and permeability values of the BIe-BIIe carbonates in the Mbuji-Mayi Supergroup.

Well	Unit	Permeability (mD)	Porosity (wt%)	Pore diameter (µm)
Stop 602	BIIe	3.45	0.85	0.01
Bena Tshovu	BIId	3.39	2.95	0.03
Kanshi#B13	BIIc	0.34	1.34	0.02
Kanshi#B13	BIIc	6.19	0.46	0.33
Kanshi#B13	BIIc	1.19	0.54	17.46
Kanshi#B13	BIIc	5.89	2.00	0.07
Kanshi#B13	BIIc	30.98	2.51	0.03
Kanshi#B13	BIIb	3.11	3.35	0.14
Bena Kalenda	BIIb	1.07	7.65	0.02
Bena Kalenda	BIIb	0.23	11.94	0.05
Tshinyama#S70	BIe	14.14	1.68	0.02
Tshinyama#S70	BIe	34.39	3.19	0.05

and DOL-II dolomites are irregular, often smooth or interlocked with concavo-convex and sutured contacts (Fig. 7A). In the mud-supported textures, the pore spaces range between 2-5 µm in diameter in DOL-I, and occasionally up to 15 µm in DOL-II. In grain-supported textures, pore spaces are dominantly interparticular (Fig. 7A) and associated with secondary vugs and fractures (Figs 7B, C, D). CAL-I to CAL-IV calcite cements (10 µm to up 200 µm) are interlocked with interparticular pore sizes of 1-2 µm on average (Fig. 7C).

Peloidal grains (DOL-IV and DOL-V) are loosely packed (Fig. 7D), and pore space range up to 30 µm. The edges of DOL-IV grains (grain sizes 30 µm to 300 µm) are smooth, angular and often corroded. Interparticular porosity of DOL-IV dolomite is poor, except in contact with other grains and cements, which are often filled by solid amorphous bitumen (Figs 7C, D). In transmitted light, the bitumen is red-brown and probably corresponds to asphaltite, although detailed analytical data are not available. DOL-IV (>20 µm) consists of tightly interlocked crystals without pore spaces.

Porosity and permeability

The porosity values of carbonates from the BIe subgroup and BII group vary between 0.8 and 11.9% (n = 12, Table 2). Pores are characterized by small mean radii ranging between 0.02 and 17.46 µm. The average porosity is ~3.2% but there are major variations in different stratigraphical intervals. The highest porosity values, up to 3%, occur in carbonates from the BIIb, BIIc and BIId subgroups.

The Mbuji-Mayi carbonate succession shows low permeability values of 0.2 – 35 mD (n = 12), with an average of 9 mD and a median value at 4 mD (Table 2). Highest permeabilities were in samples from the BIe (up to 35 mD) and BIIc (up to 31mD) subgroups.

Source rock potential

Total organic carbon (TOC) and total sulphur (TS) values

The TOC values of the samples from the BIe to BIIe subgroups range from 0.08 to 0.8% (n = 27, Table 3). The pore- and fracture-filling solid asphaltites in the BIIc subgroup have TOC values ranging between 13 and 65% wt (n = 4).

TS values (Table 3) are up to 11.5 wt% (n = 31), and the highest values occur in samples from the BIIc subgroup. Dolomitic and black shales exhibit low to moderate TS values (0.2 and 9.3 wt%; n = 11; and 0.0 and 6.4 wt% n = 3), respectively.

Carbon isotope ratios

A composite $\delta^{13}C$ profile of the Mbuji-Mayi Supergroup is shown in Fig. 8 (see data in Table 3). The BIe shaley dolostones have $\delta^{13}C$ values ranging from -28.1 ‰ to -27.4‰ (n = 4). No carbon isotopes were investigated in the BIIa dolostones. $\delta^{13}C$ values for the BIIb shaley dolostones vary between -30.2‰ and -24.7‰ (n = 5). The overlying BIIc dolostones display generally upwards-decreasing $\delta^{13}C$ values from -30.8‰ to -22.8‰ (n = 11). Three levels of black shales in the $BIIc_4$, $BIIc_6$ and $BIIc_8$ formations sampled in the Kanshi #B13 cores display $\delta^{13}C$ values between -23.0‰ and -22.8‰ (n = 3), -26.2‰ and -26.1‰ (n = 2), and -25.7‰ and -25.5‰ (n = 2). Asphaltitic dolostones in the BIIc have $\delta^{13}C$ values ranging between -32.6‰ and -28.1‰ (n = 3). Only one $\delta^{13}C$ measurement was made in the BIId dolostones and had a value of -25.2‰. Two BIIe dolomitic limestones had $\delta^{13}C$ values of -32.9‰ and -30.9‰.

Table 3. Rock-Eval pyrolysis results for black shales and organic-rich carbonates from the Mbuji-Mayi BIe-BIIe subgroups. "Asp." in the TOC column is asphaltite.

Well	Unit	$CaCO_3$ (wt%)	$\delta^{13}C$ (‰, VPDB)	TS (wt%)	TOC (wt%)	S_1 (HC g/kg)	S_2 (HC g/kg)	PI	T_{max} (°C)	HI (mgHC/g C_{org})	OI (mgHC/g C_{org})
Stop 602	BIIe	83.1	-30.9	0.01							
Stop 602	BIIe	58.9	-32.0	0.04	0.13	0.00	0.02	0.08	505	7	608
Bena Tshovu	BIId	89.4		0.04	0.04	0.00	0.02	0.05	509	45	1817
Bena Tshovu	BIId	42.2	-25.2	0.01	0.03						
Kanshi#B13	BIIc	86.7	-22.8	0.94	0.78						
Kanshi#B13	BIIc	92.6	-24.0	11.50	0.24	0.00	0.02	0.14	571	9	223
Kanshi#B13	BIIc	32.0	-24.0	0.56	0.26	0.01	0.07	0.13	411	26	179
Kanshi#B13	BIIc	16.6	-23.7	0.86	0.66	0.01	0.09	0.14	400	14	61
Kanshi#B13	BIIc	2.5	-25.5	1.35	0.23						
Kanshi#B13	BIIc	3.0	-25.7	0.17	0.16-0.21	0.01	0.03	0.16	426	21	201
Kanshi#B13	BIIc	71.1	-27.5	0.24	0.22						
Kanshi#B13	BIIc	1.5	-26.2	9.34	0.47						
Kanshi#B13	BIIc	2.4	-26.1	2.35	0.49-0.52	0.03	0.15	0.15	436	29	69
Kanshi#B13	BIIc	74.1	-28.0	4.82	0.66						
Kanshi#B13	BIIc		-28.1	3.95	***Asp.: 64.80***						
Kanshi#B13	BIIc	89.3	-28.6	0.15							
Kanshi#B13	BIIc	1.6	-22.8	4.14	0.75						
Kanshi#B13	BIIc				0.59	0.01	0.04	0.19	528	7	156
Kanshi#B13	BIIc	1.5	-23.0	0.65	0.69-0.74	0.05	0.31	0.13	405	45	157
Kanshi#B13	BIIc	2.1	-23.0	0.81	1.19						
Kanshi#B13	BIIc	86.3	-30.0	5.11							
Kanshi#B13	BIIc	91.5	-27.6	5.66	0.43						
Kanshi#B13	BIIc	84.8	-29.2	7.39							
Kanshi#B13	BIIc		-32.6	6.40	***Asp.: 57.90***						
Kanshi#B13	BIIc	84.3	-30.8	0.08	12.90						
Kanshi#B13	BIIc				***Asp.: 45.99***	0.18	0.97	0.16	364	2	7
Kanshi#B13	BIIb	71.4	-27.7	0.02	0.08						
Kanshi#B13	BIIb	77.8	-26.1	1.83	0.13	0.02	0.10	0.15	434	76	354
Kanshi#B13	BIIb	58.3	-30.2	0.07	0.33						
Bena Kalenda	BIIb	79.3	-24.7	0.04	0.44						
Bena Kalenda	BIIb	89.9	-25.1	0.16							
Bena Kalenda	BIIb				0.23	0.01	0.11	0.08	451	50	340
Tshinyama#S70	BIe		-27.7								
Tshinyama#S70	BIe	62.7	-27.4	0.89	0.33	0.02	0.15	0.12	421	46	148
Kafuku#15	BIe		-28.1								
Kafuku#15	BIe	67.5	-27.7	2.50	0.52	0.02	0.07	0.23	418	14	161

Rock-Eval pyrolysis and kerogen types

The Rock-Eval S_1 of the black shale samples analyzed ranges from 0.01 to 0.05 mg HC/g rock (n = 6), and is < 0.02 mg HC/g rock (n = 7) in the carbonates (Table 3). An asphaltite inclusion had an S_1 of 0.18 mg HC/g rock (n = 1). The S_2 of the black shales and carbonates is up to 0.31 mg HC/g rock (n = 6) and 0.15 mg HC/g rock (n = 7), respectively (Fig. 9A). S_2 for the asphaltite inclusion is 0.97 mg HC/g rock (n = 1). The production index (PI) for the black shales, dolostones, limestones and asphaltite inclusion ranges from 0.05 to 0.23 mg HC/g rock (n = 13) and 0.16 mg HC/g rock (n = 1), respectively (Fig. 9B).

The hydrogen index (HI) of the shales and the asphaltite ranges from 7 to 76 mg HC/g C_{org} (n = 13) and 2 mg HC/g C_{org} (n = 1), respectively (Fig. 9C). The oxygen index (OI) of the shales and asphaltitic dolostones ranges from 61 to 1817 mg HC/g C_{org} (n = 13) and 7 mg HC/g C_{org} (n = 1), respectively (Fig. 9C). However, the oxygen index (OI) of the black shales are slightly lower (61-201 mg HC/g C_{org}; n = 6) than in the dolostones. The T_{max} for the shales ranges from 400 to 571°C (n = 13), and is around 364°C (n=1) in the asphaltite inclusion (Fig. 9B).

Fluid inclusion thermometry

Microthermometric data are summarized in Table 4. Two-phase (liquid + vapour) inclusions (5-15 µm in diameter) are observed in saddle dolomites (DOL-IV), equant dolomites (DOL-V) and quartz (SI) cements

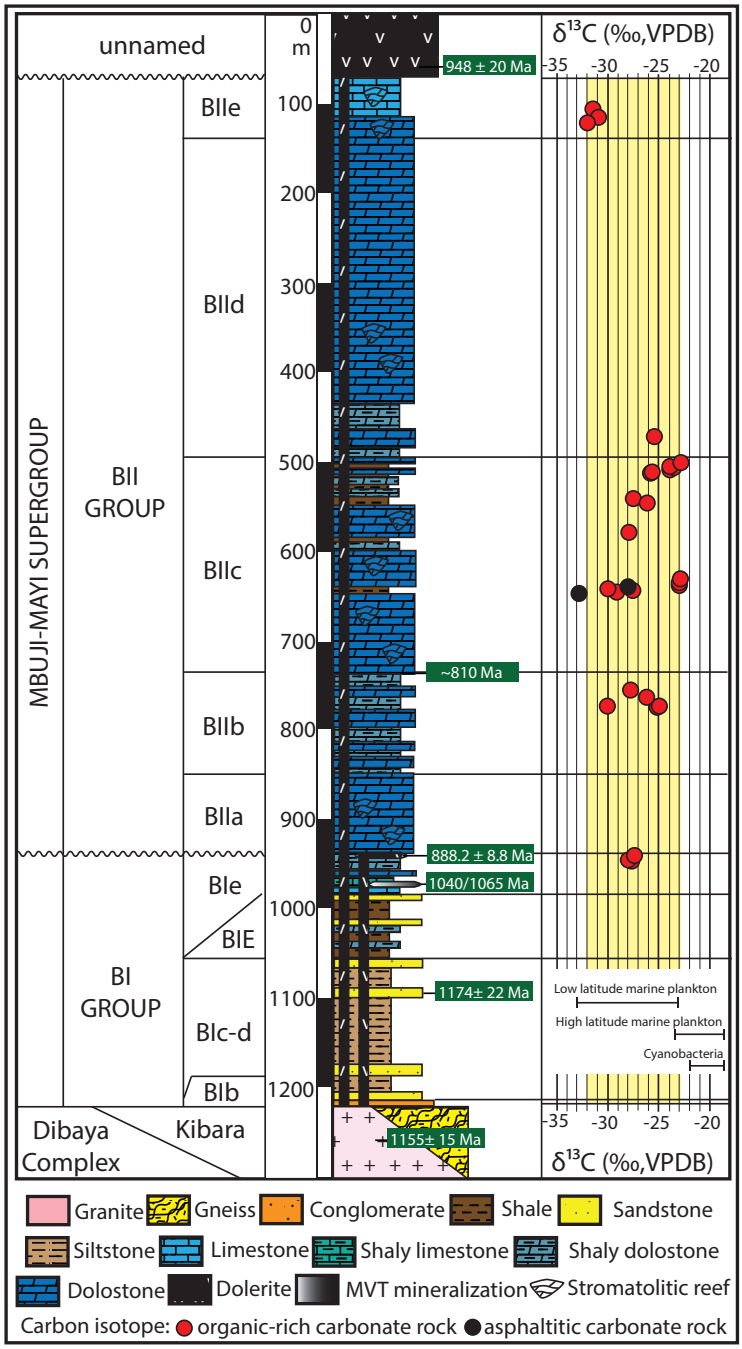

Fig. 8. Composite $\delta^{13}C$ profile of organic-rich carbonate rocks containing asphaltite inclusions in the Mbuji-Mayi Supergroup; variations are interpreted to be due to the *in situ* maturation of marine planktonic Type I/II kerogen in Meso-Neoproterozoic source rocks. The $\delta^{13}C$ values are similar to those of samples from Neoproterozoic to Palaeozoic successions (Hayes *et al.*, 1999) and to organic carbon reservoirs (Baudin *et al.*, 2007).

which fill pores and fractures in the BIIc subgroup. Primary fluid inclusions occur principally in DOL-IV and DOL-V, while secondary fluid inclusions occur in quartz. No fluid inclusions were observed in the DOL-I to DOL-III and CAL-I to CAL-IV cement phases.

The first melting temperature of primary inclusions was about -22.0°C, indicating an H_2O-NaCl system (Goldstein and Reynolds, 1994). The mean homogenization temperature is +50.6°C (n = 17) and the mean final ice melting temperature of primary inclusions is -6.2°C (n = 4) (Fig. 10). This value corresponds to a mean salinity of 9.47 wt% NaCl equiv. (Bodnar, 1993).

The first melting temperature of the secondary inclusions occurs at about -21.8°C and also indicates an H_2O-NaCl system (Goldstein and Reynolds, 1994). However, three samples have first melting temperatures between -22.0 and -22.3°C, suggesting an H_2O-NaCl-KCl system. The mean homogenization temperature ranges between +50.0 and +53.9°C (n = 8), and the mean final ice melting temperature of secondary

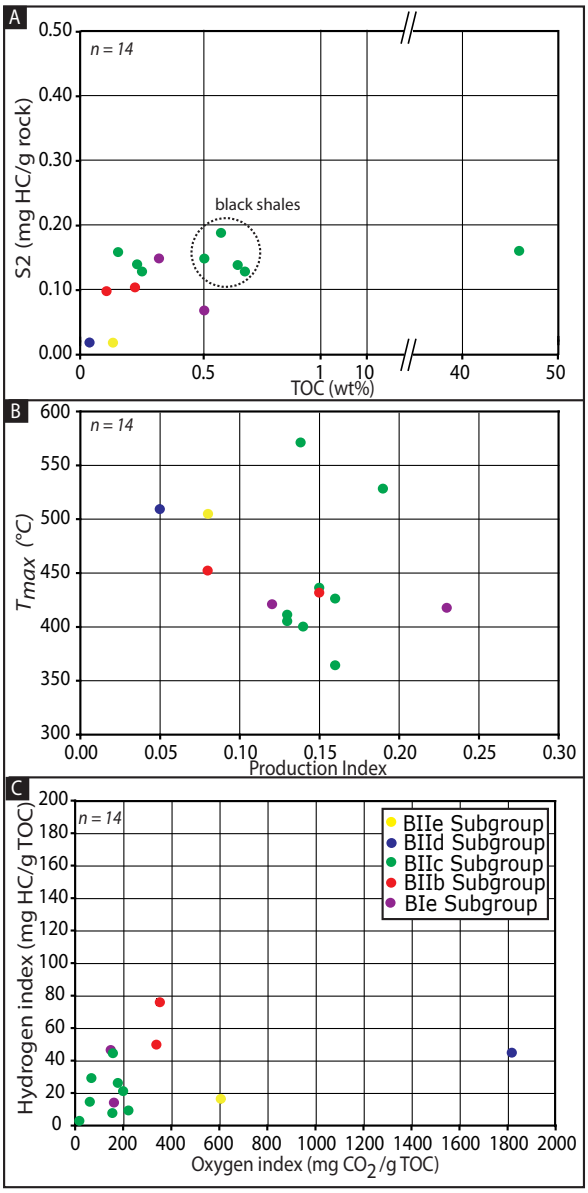

Fig. 9. Cross-plots showing the results of Rock-Eval pyrolysis of samples from the BIe-BIIe subgroups: (A) Cross-plot of Rock-Eval S_2 yield versus Total Organic Carbon (TOC) content showing a generally low source rock potential for the samples from the Mbuji-Mayi Supergroup. However, the black shales show some organic enrichment and moderate source rock potential. (B) Cross-plot of T_{max} versus production index (PI) shows a low petroleum potential; T_{max} values indicate that the samples are in the oil window. (C) Cross-plot of Hydrogen Index (HI) versus Oxygen Index (OI) showing very low HI and moderate OI values, indicating poor kerogen quality. The data-set from the Mbuji-Mayi Supergroup is similar to the data from the Neoproterozoic Alolo Subgroup and the Permo-Carboniferous Lukuga Group (see Fig. 11).

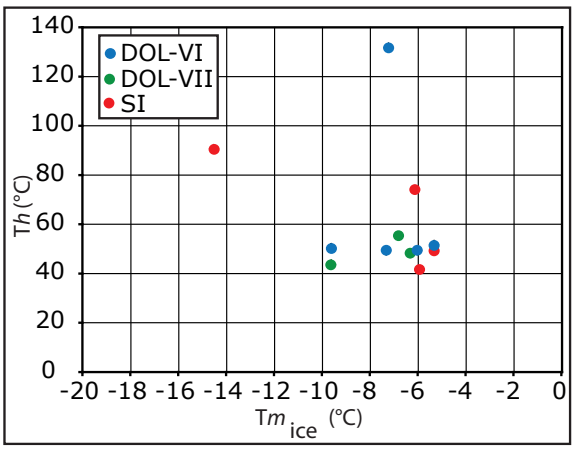

Fig. 10. Cross-plot of homogenization temperature (*Th*) versus final ice melting temperature (Tm_{ice}) for DOL-IV, DOL-V and SI crystals in dolostones from the BIIc subgroup from well Kanshi #B13 cores, showing that primary fluid inclusions correspond to an H_2O-NaCl system with a mean *Th* of +50°C (n = 12) and are related to the circulation of warm, saline (~9.5-10 wt. % NaCl equiv.) fluids in the shallow sub-surface at depths of at least 1 km (data from Delpomdor and Préat, 2012).

inclusions is -6.6°C (n = 3). This value corresponds to a mean salinity of 9.98 wt% NaCl equiv. (Bodnar, 1993).

Raman microspectroscopy on asphaltite inclusions

Asphaltite inclusions within three thin sections (BK108, BK127, BK233; BK for "Bushimay Kanshi #B13" followed by the sample number) from the BIIc subgroup from the Kanshi #B13 well cores were analyzed by Raman microspectroscopy. All samples showed spectra typical for carbonaceous material (CM) resulting from organic matter transformation/ maturation. As shown in Fig. 11, the first-order region (1000-1800 cm^{-1}) of the Raman spectra exhibits typical D and G bands which can be deconvoluted into several peaks. The deconvoluted D1 peak centre position and full-width-at-half-maximum were used to calculate maximum palaeo-temperatures (according to equation 2 in Kouketsu *et al.*, 2014). Raman reflectance $R_{mc}R_o$% – a proxy for vitrinite reflectance – was derived from the inter-peak interval (G and D_1) (c.f. Liu *et al.*, 2013).

Raman-derived palaeo-temperatures for the three samples range from ~150 to ~260°C, which is typical of low-grade metamorphism. Raman reflectance – $R_{mc}R_o$% – of samples BK108 and BK127 were 2.1-2.7%, but were lower in sample BK127 (1-1.7%). These results are consistent with previous studies on carbonaceous material in the BIe subgroup (Baludikay *et al.,* 2016a,b) which reported an average maximum palaeo-temperature of 249 ± 37°C and an average Raman reflectance of 2.01 ± 0.42 % on HF macerate residues.

Table 4. Thermometry results for bitumen inclusions in the BIIc carbonates of the Mbuji-Mayi Supergroup.

Well	Unit	Lithology	Fluid inclusion	Type	Th (°C)	Tfreez (°C)	Tfm (°C)	Tmice (°C)	Well	Unit	Lithology	Fluid inclusion	Type	T*h* (°C)	T_{freez} (°C)	T*fm* (°C)	Tm_{ice} (°C)
Kanshi#B13	BIIc	dolomite	primary	$NaCl-H_2O$	51.5				Kanshi#B13	BIIc	dolomite	unknown		48.6			
Kanshi#B13	BIIc	dolomite	primary		51.5				Kanshi#B13	BIIc	dolomite	unknown		51.8			
Kanshi#B13	BIIc	dolomite	primary		51.5				Kanshi#B13	BIIc	dolomite	unknown		36.5			
Kanshi#B13	BIIc	dolomite	primary		51.5				Kanshi#B13	BIIc	dolomite	unknown	$NaCl-H_2O$	43.5	-42.5	-21.5	-9.6
Kanshi#B13	BIIc	dolomite	primary		51.5				Kanshi#B13	BIIc	dolomite	unknown	$NaCl-H_2O$		-42.5	-21.5	-9.6
Kanshi#B13	BIIc	dolomite	primary	$NaCl-H_2O$	51.5	-49.8	-21.7	-5.3	Kanshi#B13	BIIc	dolomite	unknown		48.1	-49.6	-21.6	-6.3
Kanshi#B13	BIIc	dolomite	primary		51.5	-44.6	-22.1	-7.5	Kanshi#B13	BIIc	dolomite	unknown		66.7			
Kanshi#B13	BIIc	dolomite	primary		51.5				Kanshi#B13	BIIc	dolomite	unknown		126.0			
Kanshi#B13	BIIc	dolomite	primary		49.2				Kanshi#B13	BIIc	dolomite	unknown		131.6	-47.2	-22.4	-7.2
Kanshi#B13	BIIc	dolomite	primary		49.2				Kanshi#B13	BIIc	dolomite	unknown		57.1			
Kanshi#B13	BIIc	dolomite	primary		49.2				Kanshi#B13	BIIc	dolomite	unknown		50.2	-49.7	-21.7	-9.6
Kanshi#B13	BIIc	dolomite	primary		49.2				Kanshi#B13	BIIc	dolomite	unknown		50.2			
Kanshi#B13	BIIc	dolomite	primary		49.2	-51.3	-22.2	-6.0	Kanshi#B13	BIIc	dolomite	unknown	$NaCl-H_2O$	55.6	-48.1	-21.8	-6.8
Kanshi#B13	BIIc	quartz	secondary	$NaCl-H_2O-KCl$	90.5	-42.0	-22.3	-14.5	Kanshi#B13	BIIc	dolomite	unknown		53.5			
Kanshi#B13	BIIc	quartz	secondary		170.1				Kanshi#B13	BIIc	quartz	secondary		53.5			
Kanshi#B13	BIIc	quartz	secondary	$NaCl-H_2O-KCl$	73.9	-42.0	-22.1	-6.1	Kanshi#B13	BIIc	quartz	secondary		53.6			
Kanshi#B13	BIIc	quartz	secondary	$NaCl-H_2O$	49.1	-46.1	-20.8	-5.3	Kanshi#B13	BIIc	quartz	secondary		53.7			
Kanshi#B13	BIIc	quartz	secondary	$NaCl-H_2O$		-52.5	-21.6	-8.4	Kanshi#B13	BIIc	quartz	secondary		53.8			
Kanshi#B13	BIIc	dolomite	unknown	$NaCl-H_2O$	49.1	-46.1	-21.2	-7.3	Kanshi#B13	BIIc	quartz	secondary		53.9			
Kanshi#B13	BIIc	dolomite	unknown		49.2				Kanshi#B13	BIIc	quartz	primary	$NaCl-H_2O-KCl$	50.0	-59.2	-22.0	
Kanshi#B13	BIIc	dolomite	unknown		49.3				Kanshi#B13	BIIc	quartz	primary		41.5			
Kanshi#B13	BIIc	dolomite	unknown		49.4				Kanshi#B13	BIIc	quartz	primary	$NaCl-H_2O$	41.5	-52.1	-21.8	
Kanshi#B13	BIIc	dolomite	unknown		49.5				Kanshi#B13	BIIc	quartz	unknown		56.1	-51.8	-21.6	-5.9
Kanshi#B13	BIIc	dolomite	unknown		49.5				Kanshi#B13	BIIc	quartz	primary		63.1			

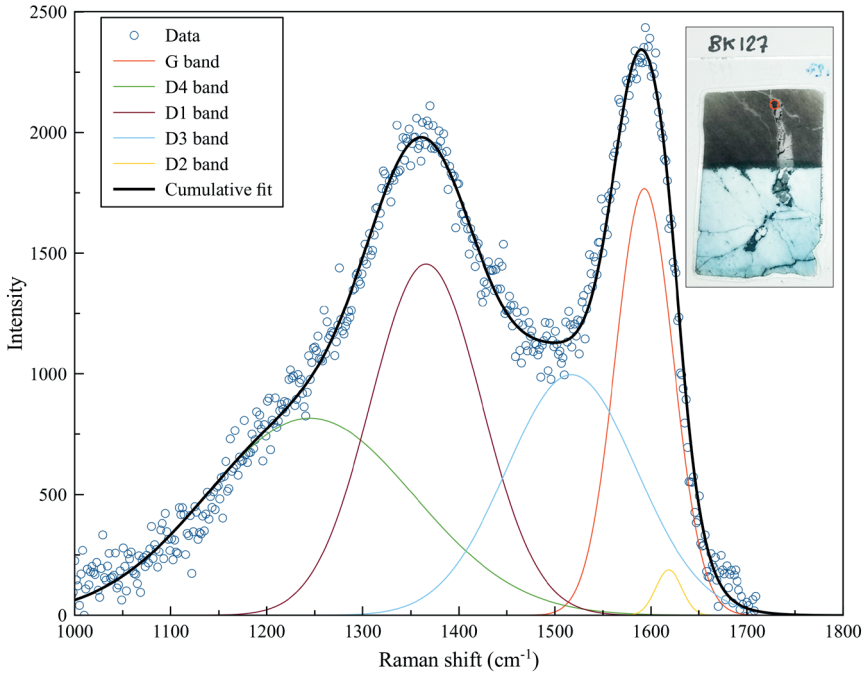

Fig. 11. Representative Raman spectrum of carbonaceous material present in a fracture in a thin section of sample BK127. The "graphite"-related G-band (~1600 cm^{-1}) is caused by the vibration of a hexagonal carbon ring structure, while the "disorder"–related D_1-band (~1350 cm^{-1}) and D_2 (1620 cm^{-1}), D_3 (1500 cm^{-1}) and D_4 (1245 cm^{-1}) are due to the amorphous nature of the carbonaceous material.

DISCUSSION

Reservoir potential

The BIe to BIIe subgroups consist of a dolomitic-shale succession recording the transition of a marine ramp from basinal and low-energy outer ramp environments, to biohermal mid-ramp oolitic shoals and restricted tide-dominated lagoon inner-ramp settings, overlain by lacustrine and sabkha environments (Delpomdor *et al.*, 2015). This results in a wide variety of dolomitic facies with both mud-supported textures (mudstones, wackestones and stromatolitic bindstones) and grain-supported textures (oolitic packstones and grainstones).

The dolo-grainstones are generally well cemented and the mud-supported textures most often exhibit partially occluded vuggy and intercrystalline microporosities. These textures are the most interesting from a reservoir point of view and the porosity is sometimes improved by fracturing. In this context, intense diagenesis has altered these muddy carbonates leading to the development of dominantly secondary fabrics. Major diagenetic processes include: (i) dissolution and/or neomorphism of probable depositional aragonite mud, as suggested by the botryoidal texture completely transformed into calcite (CAL-II); (ii) dolomitization (DOL-I and DOL-II); (iii) calcite cementation (CAL-I to CAL-IV); (iv) mechanical compaction and pressure solution; (v) fracturing; (vi) further dolomite cementation (DOL-III to DOL-V); (vii) generation and migration of oil and bitumen; (viii) dissolution and silicification; and (ix) dedolomitization with calcite cementation. Fig. 5 summarizes the sequence of these diagenetic processes based on the petrographic observations.

Synsedimentary dolomitization may have occurred before the conversion of aragonite to calcite (Hood *et al.*, 2011). Calcite matrix material has not been observed as a result of the dolomitization. However, in thin sections, the recrystallized textures (mimic DOL-I and DOL-II) suggest an originally aragonitic muddy precursor, which underwent alteration as a result of dolomitizing fluids derived from lagoons and pools associated with the sabhka evaporites (ANH-I) (Delpomdor *et al.*, 2015). Porosity in the mudstones was low, except in the oolitic and stromatolitic carbonates which have higher primary porosity. However, the observation of subaerial exposure surfaces suggests that secondary porosity has been occluded by meteoric calcite cements, which were replaced by the DOL-III cements. Other calcite cements have occluded substantial amounts of porosity in the Mbuji-Mayi carbonates, and filled intergranular pore spaces and reefal cavities. These cement types are common in open-marine seafloor sediments and filled reefal cavities in stromatolitic build-ups during the Neoproterozoic (Sumner, 1997).

The iron-rich CAL-I to CAL-IV calcite cements observed in the vugs may record reducing conditions related to bacterial sulphate reduction near the shale-rich intervals (Sumner, 1997). DOL-III to DOL-V cements in pore spaces and fractures formed during intermediate and late diagenesis, and were related to

phases of regional uplift resulting in fluid circulation (Delpomdor and Préat, 2012). Saddle dolomite (DOL-IV) is commonly associated with deep burial settings (Radke and Mathis, 1980) and hydrothermal activity. Precipitation from saline brines led to the formation of evaporite cements (ANH-II) in fractures, and is often accompanied by lead-zinc mineralization as locally observed in the SMLL Basin (Polinard, 1929).

Primary porosity in the aragonitic and DOL-I to -II matrices was therefore relatively low, but secondary porosity in DOL-III to -IV reaches 11.9%. This was related to fracturing and the dissolution of carbonate grains and matrix during DOL-V cementation and later silicification. Compaction of the muddy deposits during burial may also explain the relatively poor porosity and permeability of the carbonates. The low porosity (av. ~3.2%) and permeability (0.22-34.68 mD) of these rocks prevent them from having the potential to be effective conventional reservoirs for oil and gas. However, the presence of solid asphaltite (Figs 7B, C and D) in the fractures associated with the DOL-IV and -V phases record the formation and migration of liquid oil from mature source rocks.

Source rock potential

TOC values of the studied black shales and organic rich-carbonates analyzed suggest that they have poor source rock potential, with TOC values ranging between 0.5 and 1%, although rocks with 0.5-1% TOC values can be classified as marginal source rocks. The presence of solid asphaltite in inclusions suggests that maturation of oil-prone source rocks has occurred.

The TS values are in general low, suggesting a low consumption of sulphur from organic matter under oxic marine to lacustrine conditions. However, high TS values associated with the higher TOC values in the BIIc black shale samples may indicate preservation of the organic matter in anoxic bottom waters. An adequate nutrient supply is indicated by the abundance of microorganisms in the shales. The TS values are indicative of the intensity of bacterial sulphate reduction, which is related to the quantity and reactivity of the organic matter entering the anoxic zone (Berner, 1970, 1984). Under anoxic conditions, dissolved sulphate is reduced to H_2S which reacts with iron materials to form iron sulphides (Canfield and Raiswell, 1991). Low TOC values and high TS are characteristic of strong bacterial sulphate reduction, while high TOC values and low TS values suggest a weak consumption of sulphur in the organic matter and therefore point to oxic conditions (Berner, 1970, 1984).

The analyzed black shales and organic rich-carbonates have low source rock potential (Rock-Eval S_2: 0.03 to 0.31 mg HC/g rock). The PI is low as S_1 and S_2 values are very low. The OI is high while HI is low. An HI versus OI plot of the studied black shales

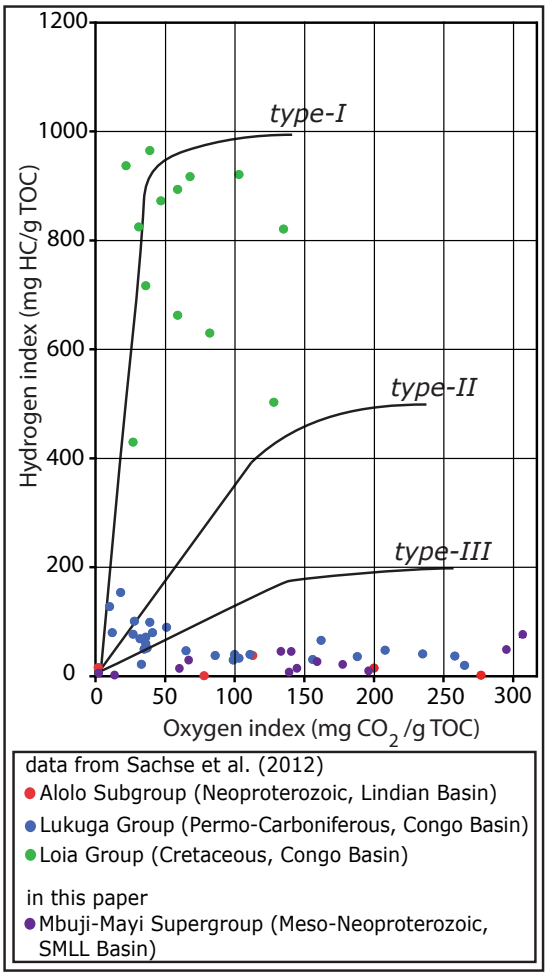

Fig. 12. Cross-plot of hydrogen Index (HI) versus oxygen index (OI) showing the kerogen quality of samples from the BIe-BIIe subgroups compared to that of Neoproterozoic Alolo Subgroup black shales from the Lindian Basin, and black shales from the Permo-Carboniferous Lukuga Group and the Cretaceous Loia Group in the Congo Basin. Data for the samples from the Alolo subgroup and Lukuga and Loia Groups are from Sachse *et al.* (2012). Kerogen from the Precambrian and Palaeozoic rocks has poor source rock potential (Type IV).

and organic-rich carbonates indicates Type IV kerogen (Fig. 12), with little conventional potential. T_{max} values are in general below 435 °C (n = 8) and indicate thermal immaturity (Peters, 1986; Pratt *et al.*, 1988). However, the Raman spectroscopy data on asphaltite inclusions (which are consistent with previous Raman data on HF macerates of eu- and prokaryotic organic matter from the Mbuji-Mayi Supergroup; Baludikay *et al.*, 2016b) indicate palaeotemperatures ranging from 160 to 260˚C, and Raman reflectance ($R_{mc}R_o$%) ranging from 1.05 to 2.57 %. This suggests that the organic matter from the Mbuji-Mayi Supergroup is likely in a maturation stage corresponding to the oil and wet gas window. Oil window maturation, followed by primary oil migration, occurred during the Lufilian deformation phase (660-530 Ma) (Kipata *et al.*, 2013).

Similar low TOC contents, Type IV kerogens and moderate to high thermal maturities have been reported in the Neoproterozoic Alolo Shale Subgroup in the DR Congo (Sachse *et al.*, 2012; Fig. 12), and in the Riphean Vedreshev and Madrin Formations in Russia (Filiptsov *et al.*, 1999).

Origin of the asphaltite

The origin of the asphaltite in the Bllc carbonates appears to be associated with other potential source rocks in the SMLL and adjacent basins. These include the Mid-Neoproterozoic organic-rich carbonates of the Kakontwe Formation of the Katanga Basin, which contain residues of shungite (amorphous, ungraphitized organic material: Heijlen *et al.*, 2008); the Permo-Carboniferous peri-glacial shales of the Lukuga Group and the Lower Jurassic black argillites of the Stanleyville Group, which are present in the Congo Basin; and the Lower Cretaceous organic-rich argillites of the Loia Group which occur in both the SMLL and Congo Basins.

Carbon isotope studies may provide some information about the origin of the asphaltite. However, $\delta^{13}C$ values of asphaltite depend on both the $\delta^{13}C$ values of the kerogen in the associated source rocks and on the physical and chemical processes involved in asphaltite formation and alteration. In this study, the $\delta^{13}C$ values of the solid asphaltites had a narrow range (up to 5‰) and were similar to the $\delta^{13}C$ values of samples from the Mbuji-Mayi Supergroup (Fig. 8). These $\delta^{13}C$ values may indicate *in situ* maturation of marine planktonic organic matter in the Neoproterozoic source rocks in the Supergroup. Alternatively, they may indicate downward migration of hydrocarbons derived from terrigenous plant material in the Permo-Carboniferous coals of the Lukuga Group, as occurs in the north Katanga Basin. The hydrocarbons may also have been sourced from Mesozoic argillites of the Stanleyville and Loia Groups, as occurs in the Congo Basin. However, no oil seeps derived from source rocks in the Lukuga and Loia Groups have been identified in the SMLL Basin. The low T_{max} (364°C) of the asphaltites indicates the immaturity of the organic material, while the T_{max} of the OM in the Meso-Neoproterozoic, Permo-Carboniferous and Lower Cretaceous sucessions is 400-450°C (Sachse *et al.*, 2012; Delvaux and Fernandez-Alonso, 2015). Local high T_{max} values (>500°C) may be due to thermal maturation associaed with local volcanism; for example, lava flows are in contact with the Mbuji-Mayi carbonates around Mbuji-Mayi town.

In the Katanga Basin, the asphaltite is considered to have formed during regional uplift related to the effects of the Lufilian deformation (650-530 Ma; Kipata *et al.,* 2013), and to be associated with thermochemical sulphate reduction (e.g. at temperatures of 290-380°C) during the Cambro-Ordovician (~540-480 Ma) (Schneider *et al.*, 2007; Heijlen *et al.*, 2008). This process reduced the carbon content leading to the formation of shungite fragments and globules which represent a thermally-altered precursor petroleum (Heijlen *et al.*, 2008). The SMLL Basin was affected by time-equivalent upward migration of saline fluids which resulted in precipitation of ANH-II in the fractures in the BII carbonates; the saline fluids expelled oil residues from the source rocks as immature oil. The expelled oil was probably altered through natural processes such bacterial degradation under aerobic conditions at shallow depths (less than 1 km) and temperatures < 80°C. These conditions are supported by the thermal analyses in the fluid inclusions of the late cements (DOL-IV, DOL-V and SI) suggesting circulation of slightly saline fluids (~9.5-10 wt. % NaCl equiv.) at depths of <1km and temperatures at or below +50°C.

In conclusion, the presence of asphaltite is indicative of the biodegradation of immature oil derived from marine planktonic (Type I/II) kerogen, which underwent secondary migration probably during the Cambro-Ordovician (~540-480 Ma).

Regional petroleum potential

The black shales in the BIIc subgroup, with TOC values of 1 wt%, low HI and moderate OI values, have a wide distribution, estimated at 3 x 10^6 km^2 and cover much of the SMLL Basin, probably extending into the southern part of the Congo Basin. The carbonates and black shales in the Mbuji-Mayi Supergroup were deposited between 1000 and 800 Ma (Delpomdor *et al.*, 2013, Baludikay *et al.*, 2016a). Maturation of Type I/II kerogen and primary oil migration is interpreted to have occurred during Lufilian deformation (660-530 Ma; Kipata *et al.*, 2013), while secondary oil migration probably occurred at ~540-480 Ma and may have been related to uplift associated with the paroxysmal phase of Lufilian deformation in the Katanga Basin. The solid asphaltite in the fractured dolostones in the Mbuji-Mayi Supergroup is considered to be coeval with the shungite in the Kakontwe Formation in the Katanga Basin. This last phase of oil migration, evidenced by the presence of solid asphaltite in pores and fractures associated with inclusion-fluid-rich cements (DOL-IV, DOL-V and SI), was related to the circulation of warm (+50°C), saline (~9.5-10 wt. % NaCl equiv.) fluids at shallow depths of at least 1 km. Although this study presents new data on the SMLL Basin, the petroleum system is still largely unknown.

CONCLUSIONS

Carbonate samples, source rocks and asphaltites from the Meso-Neoproterozoic Mbuji-Mayi Supergroup

in the Sankuru-Mbuji-Mayi-Lomami-Lovoy Basin (south-central Democratic Republic of Congo) were analyzed to evaluate potential reservoir and source rocks. Results show that carbonate rocks have relatively poor reservoir potential with porosity up to 12% in secondary vugs and fractures. Potential source rocks have low organic matter content (TOC values <1.19%, and <0.78% for black shales and organic-rich carbonates, respectively) and appear to have little potential for conventional oil and gas generation based on Rock-Eval pyrolysis. The dominant kerogen type in both black shales and carbonates is Type IV, derived from Type I/II kerogen from marine and lacustrine acritarchs and cyanobacteria. Asphaltite filling secondary vugs and fracture porosity appears to have been derived initially from a single genetic group of Type I/II kerogen based on bulk carbon isotopic ratios.

The $\delta^{13}C$ values of the solid asphaltites (-32.6 to -28.1‰) were similar to the $\delta^{13}C$ values (-30.2 to 22.8‰) of organic-rich carbonate rocks from the Mbuji-Mayi Supergroup, which may indicate *in situ* maturation of marine planktonic organic matter. The thermal maturity of asphaltite inclusions in carbonate samples is indicated by Raman-spectroscopy derived palaeo-temperatures ranging from ~150 to ~260°C, which is typical of low-grade metamorphism. Raman reflectance ($R_{mc}R_o$%) values for the asphaltite were between 1.0 and 2.7%, indicating mature organic matter corresponding to the oil and wet gas windows. Maturation and primary oil migration are interpreted to have occurred during Lufilian deformation (650-530 Ma. Asphaltite formation occurred during the Cambrian-Ordovician (~540-480 Ma) and may have been related to uplift associated with the paroxysmal phase of the Lufilian deformation in the Katanga Basin to the SE.

Based on the evidence presented, the Mbuji-Mayi succession may show significant indications for an active petroleum system during the Late Neoproterozoic and Early Palaeozoic. The environment of deposition together with diagenetic processes (and fracturing) in the Meso-Neoproterozoic succession were favourable for oil entrapment. The history of oil migration is linked to multiple tectonic events which have affected the SMLL and the adjacent basins. Current knowledge of the petroleum system in the greater Congo Basin area is limited which precludes the prediction of viable hydrocarbon resources. This study is intended to provide a starting-point for future hydrocarbon exploration in this area.

ACKNOWLEDGEMENTS

The authors acknowledge the Royal Museum for Central Africa (RMCA, Belgium) for kindly granting access to the samples from the Mbuji-Mayi Supergroup, and TOTAL S.A. for the Rock-Eval analysis. We thank JPG editorial staff and reviewer Victoria Sachse (RWTH Aachen University) for thoughtful and constructive comments and suggestions which improved the manuscript significantly.

REFERENCES

BALUDIKAY, B.K., STORME, J.-Y., BAUDET, D., FRANÇOIS, C. and JAVAUX, E.J., 2016a. A diverse and exquisitely preserved organic-walled microfossil assemblage from the Meso-Neoproterozoic Mbuji-Mayi Supergroup (Democratic Republic of Congo) and implications for Proterozoic biostratigraphy. *Precambrian Research*, **281**, 166-184.

BALUDIKAY, B.K., STORME, J.-Y., BAUDET, D., FRANÇOIS, C. and JAVAUX, E.J., 2016b. Thermal maturation of carbonaceous material from Mbuji-Mayi Supergroup (Kasaï, Democratic Republic of Congo). Vienna, European Geosciences Union, *Geophysical Research Abstracts*, **18**, EGU2016-4574.

BAUDET, D., 1987. Implications of a palynological study in the Upper Precambrian from eastern Kasaï and nortwestern Shaba, Zaïre. *Geology Journal*, **22**, 121-137.

BAUDIN, F., TRIBOVILLARD, N. and TRICHET, J., 2007. Géologie de la matière organique. Société Géologique de France, Vuibert, 260 p.

BERNER, R.A., 1970. Sedimentary pyrite formation. *American Journal of Science*, **268**, 1-23.

BERNER, R.A., 1984. Sedimentary pyrite formation: an update. *Geochimica et Cosmochimica Acta,* **48,** 605-615.

BERTRAND-SARFATI, J., 1972. Stromatolithes columnaires de certaines formations carbonatées du Précambrien supérieur du basin congolais (Bushimay, Lindien, Ouest-Congolien). *Annales du Musée Royal de l'Afrique Centrale, Tervuren, Belgique, Série in-8*, **74**, 45 pp.

BODNAR, R.J., 1993. Revised equation and table for determining the freezing point depression of H_2O-NaCl solutions. *Geochimica et Cosmochimica Acta,* **57**, 683-684.

BONNEVILLE, S., BAERT, K., HUBIN, A. and DELPOMDOR, F., 2015. In Search of Neoproterozoic Fungi Microfossils. Prague, Czech Republic, 25th Goldschmidt.

CAHEN, L., 1954. Extension et âge d'une minéralisation Cu, Pb, Zn en Afrique centrale et australe. *Bulletin Société belge, Géologie, Hydrologie, Paléontologie*, **63**, 89–100.

CAHEN, L. and MORTELMANS, G., 1947. Le système de la Bushimaie au Katanga. *Bulletin Société belge, Géologie, Hydrologie, Paléontologie*, **56**, 217-253.

CAHEN, L., FERRAND, J.J., HAARSMA, M.J.F., LEPERSONNE, J. and VERBEEK, T., 1959. Description du sondage de Samba. *Annales du Musée royal du Congo belge in-8, Science Géologique*, **29**, 210 pp.

CAHEN, L., FERRAND, J.J., HAARSMA, M.J.F., LEPERSONNE, J. and VERBEEK, T., 1960. Description du sondage de Dekese. *Annales du Musée royal du Congo belge in-8, Science Géologique,* **34**, 215 pp.

CAHEN, L., LEDENT, D. and SNELLING, N.J., 1974. Données géochronologiques dans le Katanguien inférieur du Kasaï oriental et du Shaba nord-oriental (République du Zaïre). Musée Royal Afrique Centrale, Tervuren, Rapport annuel Département Géologie Mines, p. 59-70.

CAHEN, L., SNELLING, N.J., DELHAL, J. and VAIL, J.R., 1984. Geochronology and Evolution of Africa. Clarendon Press, Oxford, 512 pp.

CANFIELD, D. E. and RAISWELL, R., 1991. Pyrite formation and fossil preservation. In: ALLISON, P.A. and BRIGGS, D.E.G. (Eds.). Taphonomy. Releasing the data locked in the fossil record. New York, Plenum Press, pp. 337- 387.

COLIN, J.-P., 1994. Mesozoic-Cenozoic lacustrine sediments of

the Zaïre Interior Basin. In: GIERLOWSKI-KORDESCH, E. and KELTS, K. (Eds.). Global geological record of lake basins. Cambridge, Cambridge University Press, p. 31-36.

DALY, M.C., LAWRENCE, S.R., DIEMU-TSHIBAND, K. and MATOUANA, B., 1992. Tectonic evolution of the Cuvette Centrale, Zaïre. *Journ. Geol. Soc. Lond.*, **149**, 539–546.

DELHAL, J. and LADMIRANT, H., 1979. Carte géologique à l'échelle du 1/200.000. Notice explicative de la feuille Mbuji Mayi (degré carré S7/23 = SB34.18). Kinshasa, Département des Mines, Direction de la Géologie, 50 p.

DELHAL, J., LEPERSONNE, J. and RAUCQ, P., 1966. Le Complexe sédimentaire et volcanique de la Lulua (Kasaï). *Annales Musée Royal Afrique Centrale, Tervuren*, **51**, 106 p.

DELPOMDOR, F. and PRÉAT, A., 2012. Hydrocarbon reservoir potential of Neoproterozoic carbonates in the Mbuji-Mayi Supergroup (Sankuru-Bushimay area), Democratic Republic of Congo. Stratigraphy, sedimentology, geochemistry, petrophysics. Brussels, Université libre de Bruxelles, *confidential report*, 276 p.

DELPOMDOR, F. and PRÉAT, A., 2013. Early and late Neoproterozoic C, O and Sr isotope chemostratigraphy in the carbonates of West Congo and Mbuji-Mayi supergroups: A preserved marine signature? *Palaeogeography, Palaeoclimatology, Palaeoecology,* **389**, 35-47.

DELPOMDOR, F., BLANPIED, C., VIRGONE, A. and PRÉAT, A., 2013a. Paleoenvironments in Meso–Neoproterozoic carbonates of the Mbuji-Mayi Supergroup (Democratic Republic of Congo)–Microfacies analysis combined with C–O–Sr isotopes, major-trace elements and REE+ Y distributions. *Journal of African Earth Sciences*, **88**, 72-100.

DELPOMDOR, F., LINNEMANN, U., BOVEN, A., GÄRTNER, A., TRAVIN, A., BLANPIED, C., VIRGONE, A. and PRÉAT, A., 2013b. Depositional age, provenance, and tectonic and paleoclimatic settings of the late Mesoproterozoic–middle Neoproterozoic Mbuji-Mayi Supergroup, Democratic Republic of Congo. *Palaeogeography, Palaeoclimatology, Palaeoecology*, **389**, 4-34.

DELPOMDOR, F., BLANPIED, C., VIRGONE, A. and PRÉAT, A., 2015. Sedimentology and Sequence Stratigraphy of the Late Precambrian Carbonates of the Mbuji-Mayi Supergroup in the Sankuru-Mbuji-Mayi-Lomami-Lovoy Basin (Democratic Republic of the Congo). In: DE WIT, M.J., GUILLOCHEAU, F. and DE WIT, M.C.J. (Eds.). Geology and Resource Potential of the Congo Basin. Amsterdam, Springer-Verlag, p. 59-76.

DELVAUX, D and FERNANDEZ-ALONSO, M., 2015. Petroleum Potential of the Congo Basin. In: DE WIT, M.J., GUILLOCHEAU, F. and DE WIT, M.C.J. (Eds), Geology and Resource Potential of the Congo Basin. Amsterdam, Springer-Verlag, pp. 371-391.

DEMAIFFE, D. and FIEREMANS, M., 1981. Strontium-isotopic geochemistry of the Mbuji Mayi and Kundelungu kimberlites (Zaïre, Central Africa). *Chemical Geology*, **31**, 311-323.

DEMAIFFE, D., FIEREMANS, M. and FIEREMANS, C., 1991. The kimberlites of Central Africa: a review. In: KAMPUNZU, A.B. and LUBALA, R.T. (Eds), Magmatism in Extensional Structural Settings: the Phanerozoic African Plate. New York, Springer-Verlag, p. 537–559.

ESPITALIÉ, J., DEROO, G. and MARQUIS, F., 1985. Rock-Eval pyrolysis and its applications, part I. *Revue Institut Français Pétrole,* **40**, 563–579.

FIEREMANS, C., 1977. Mode of occurrence and tectonic control of the kimberlite bodies in east Kasaï (Zaïre). Santa Fe, New Mexico, Extended Abstract 2nd International Kimberlite Conference.

FILIPTSOV, Y.A., PETRISHINA, Y.V., BOGORODSKAYA, L.I., KONTOROVICH, A.A. and KRININ, V.A., 1999. Evaluation of maturity and oil- and gas-generation properties of organic matter in Riphean and Vendian rocks of the Baykit and Katanga petroleum regions. *Geologiya i Geofizika*, **40** (9), 1362–1374.

FITZSIMONS, I.C.W., 2000. A review of tectonic events in the East Antarctic shield, and their implications for Gondwana and earlier supercontinents. *Journal of African Earth Sciences*, **31**, 3–23.

FRANÇOIS, C., BALUDIKAY, B.K., STORME, J.-Y., BAUDET, D., PAQUETTE, J.L., FIALIN, M. and JAVAUX, E.J., 2017. Contributions of U-Th-Pb dating on the diagenesis and sediment sources of the lower group (BI) of the Mbuji-Mayi Supergroup (Democratic Republic of Congo). *Precambrian Research*, **298**, 202-219.

GOLDSTEIN, R.H. and REYNOLDS, T.J., 1994. Systematics of fluid inclusions in diagenetic Minerals. Society for Sedimentary Geology *Short Course*, **31**, 199 pp.

HAYES, J.M., STRAUSS, H. and KAUFMAN, A.J., 1999. The abundance of ^{13}C in marine organic matter and isotopic fractionation in the global biogeochemical cycle of carbon during the past 800 Ma. *Chemical Geology,* **161**, 103–126.

HEINE, C., ZOETHOUT, J. and MÜLLER, R.D., 2013. Kinematics of the South Atlantic rift. *Solid Earth* 4, 215–253.

HEIJLEN, W., BANKS, D.A., MUCHEZ, P., STENSGARD, B.M. and WARDLEY, B.W.D., 2008. The Nature of Mineralizing Fluids of the Kipushi Zn-Cu Deposit, Katanga, Democratic Republic of Congo: Quantitative Fluid Inclusion Analysis using Laser Ablation ICP-MS and Bulk Crush-Leach Methods. *Economic geology*, **103**, 1459-1482.

HOLMES, A. and CAHEN, L., 1955. African geochronology. *Colonial Geology and Mineral Resources*, **5**, 3-38.

HOOD. A.S., WALLACE, M.W. and DRYSDALE, R.N., 2011. Neoproterozoic aragonite dolomite seas? Widespread marine dolomite precipitation in Cryogenian reef complexes. *Geology*, **39**, 871–874.

JNOC, 1984. Rapport des investigations géophysiques et géologiques dans la Cuvette centrale de la République du Zaïre. Japan National Oil Corporation, *unpublished report*, 205 p.

KADIMA, E.K., NTABWOBA, S.M.S. and LUCAZEAU, F., 2011a. A Proterozoic-rift origin for the structure and the evolution of the Congo basin. *Earth Planetary Science Letters*, **304,** 240-250.

KADIMA, E., DELVAUX, D., SEBAGENZI, S.N., TACK, L. and KABEYA, M., 2011b. Structure and geological history of the Congo Basin: An integrated interpretation of gravity, magnetic and reflection seismic data. *Basin Research,* **23** (5), 499-527.

KADIMA KABONGO, E., DELVAUX, D., EVERAERTS, M., SEBAGENZI, M.N.S. and LUCAZEAU, F., 2015. Neoproterozoic to Lower Paleozoic Sequences of the Congo Shield: Comparisons Between the Congo and its Peripheral Basins. In: DE WIT, M.J., GUILLOCHEAU, F. and DE WIT, M.C.J. (Eds.). Geology and Resource Potential of the Congo Basin. Amsterdam, Springer-Verlag, pp. 97-109.

KIPATA. M.L., DELVAUX, D., SEBAGENZI, M.N., CAILTEUX, J. and SINTUBIN, M., 2013. Brittle tectonic and stress field evolution in the Pan-African Lufilian Arc and its foreland (Katanga, DRC): from orogenic compression to extensional collapse, transpressional inversion and transition rifting. *Geologica Belgica,* **16**, 1-17

KOUKETSU, Y., MIZUKAMI, T., MORI, H., ENDO, S., AOYA, M., HARA, H., NAKAMURA, D. and WALLIS, S., 2014. A new approach to develop the Raman carbonaceous material geothermometer for low-grade metamorphism using peak width. *Island Arc*, **23**, 33–50.

LAWRENCE, S.R. and MAKAZU, M.M., 1988. Zaïre's Central Basin: prospectivity outlook. *Oil and Gas Journal,* **86**, 105-108.

LINOL, B., DE WIT, M.J., BARTON, E., GUILLOCHEAU, F., DE WIT, M.C.J. and COLIN, J.-P., 2015. Facies Analysis, Chronostratigraphy and paleo-environmental reconstructions of Jurassic to Cretaceous sequences of the Congo Basin. In: DE WIT, M.J., GUILLOCHEAU, F. and DE WIT, M.C.J. (Eds), Geology and Resource Potential of

the Congo Basin. Amsterdam, Springer-Verlag, pp. 135-161.
LIU, Y., ZHANG, C., SHEN, X., ZHANG, X., CICHELLO, S., GUAN, H. and LIU, P., 2013. Microorganism lipid droplets and biofuel development. *BMB Rep.*, **46** (12), 575-81.
MAHESHWARI, H.K., BOSE, M.N. and KUMARAN, K.P.N., 1977. Mesozoic sporae dispersae from Zaïre. III. Some miospores from the Stanleyville Group. *Koninklijk Museum voor Midden-Afrika Annalen, Reeks in 8°, Geologische Wetenschappen,* **80,** 45-60.
MAITHY, P.K., 1975. Micro-organisms from the Bushimay system (Late Precambrian) of Kanshi, Zaïre. *The Paleobotanist,* **22,** 133-149.
MEERT, J.G., 2003. A synopsis of events related to the assembly of eastern Gondwana. *Tectonophysics,* **362**, 1–40.
MELLO, M.R., 2008. Field survey, seep collection and HRGT analysis of seeps over CoMiCo exploration areas and samples correlation with Brazil, Africa and Middle-East. High Resolution Technology & Petroleum (HRT), *unpublished report,* 130 p.
MOUNDOUNGA, G., 2008. Sub-Saharan Africa. Democratic Republic of Congo. *GEPS Reports*, IHS, 25 p.
PETERS, K.E., 1986. Guideline for evaluation petroleum source rocks using programmed pyrolysis. *AAPG Bulletin*, **70**, 318-328.
POLINARD, E., 1929. Les gisements plombo-cuprifères de la Lubi et de la Lukala. Leur genèse et leurs rapports avec la stratigraphie de la région. *Annales Société Géologie Belgique, Publication relative au Congo belge,* **48,** 41-123.
PRATT, L.M., SHAW, C.A. and BURRUSS, R.C., 1988. Thermal history of the Hartford and Newark basins infereed from maturation indices of organic matter. In: FROELICH, A.J. and ROBINSON, G.R. (Eds), Studies of the early Mesozoic basins of the United States. U.S. Geological Survey Bulletin, 1776, pp. 58-63.
RADKE, B.M. and MATHIS, R.L., 1980. On the formation and occurrence of saddle dolomite. *Journal of Sedimentary Petrology,* **50**, 1149-1168.
RAUCQ, P., 1957. Contribution à la reconnaissance du Système de la Bushimay. *Annales Musée Royal Congo belge, Tervuren, Belgique, Série in-8°,* **18,** 427 p.
RAUCQ, P., 1970. Nouvelles acquisitions sur le système de la Bushimay (République Démocratique du Congo). *Annales Musée Royal Afrique Centale, Tervuren, Belgique, Série in-8°*, **69**, 434 p.
SACHSE, V.F., DELVAUX, D. and LITTKE, R., 2012. Petrological and geochemical investigations of potential source rocks of the central Congo Basin, Democratic Republic of Congo. *AAPG Bulletin*, **96**, 245-275.
SCHNEIDER, J., MELCHER, F. and BRAUNS, M., 2007. Concordant ages for the giant Kipushi base metal deposit (DRC) from direct Rb-Sr and Re-Os dating of sulfides. *Mineralium Deposita*, **42**, 791–797.
SUMNER, D.Y., 1997. Carbonate precipitation and oxygen stratification in late Archean seawater as deduced from facies and stratigraphy of the Gamohaan and Frisco Formations, Transvaal Supergroup, South Africa. *American Journal Science*, **297**, 455–487.
SUMNER, D.Y. and GROTZINGER, J.P., 1996. Herringbone calcite, petrography and environmental significance. *Journal of Sedimentary Research*, **66**, 419-429.
TACK, L., WINGATE, M.T., LIÉGEOIS, J.-P., FERNANDEZ-ALONSO, M. and DEBLOND, A., 2001. Early Neo-proterozoic magmatism (1000-910 Ma) of the Zadinian and Mayumbian Groups (Bas-Congo): onset of Rodinia rifting at the western edge of the Congo craton. *Precambrian Research*, **110,** 277-306.
TISSOT, B.P. and WELTE, D.H., 1984. Petroleum formation and occurrence. Berlin, Springer-Verlag, 699 p.
TORSVIK, T.H. and COCKS, L.R., 2011. The Palaeozoic paleogeography of central Gondwana. In: VAN HINSBERGEN, D. J. J., BUITER, S.J.H., TORSVIK, T.H., GAINA, C. and WEBB, S.J. (Eds), The formation and evolution of Africa: a synopsis of 3.8 Ga of Earth history. *Geol. Soc. Lond., Spec. Publ.*, 137-166.
WOIDYR, M.F., 2010. A general-purpose peak fitting program, *Journal of Applied Crystallography,* **43**, 1126-1128.